Title

Vesicle encapsulation stabilizes intermolecular association and structure formation of functional RNA and DNA

Journal

Current Biology, 32(1)

ISSN

0960-9822

Authors

Peng, Huan
Lelievre, Amandine
Landenfeld, Katharina
et al.

Publication Date

2022

DOI

10.1016/j.cub.2021.10.047

Peer reviewed

HHS Public Access

Author manuscript

Curr Biol. Author manuscript; available in PMC 2023 January 10.

Published in final edited form as:

Curr Biol. 2022 January 10; 32(1): 86–96.e6. doi:10.1016/j.cub.2021.10.047.

Vesicle encapsulation stabilizes intermolecular association and structure formation of functional RNA and DNA

Huan Peng[1], **Amandine Lelievre**[2], **Katharina Landenfeld**[2], **Sabine Müller**[2], **Irene A. Chen**[1,*]

[1]Department of Chemical and Biomolecular Engineering, University of California, Los Angeles, CA 90095, USA

[2]Institute of Biochemistry, University of Greifswald, 17487 Greifswald, Germany

Summary

During the origin of life, encapsulation of RNA inside vesicles is believed to have been a defining feature of the earliest cells (protocells). The confined biophysical environment provided by membrane encapsulation differs from that of bulk solution, and has been shown to increase activity as well as evolutionary rate for functional RNA. However, the structural basis of the effect on RNA has not been clear. Here, we studied how encapsulation of the hairpin ribozyme inside model protocells affects ribozyme kinetics, ribozyme folding into the active conformation, as well as cleavage and ligation activities. We further examined the effect of encapsulation on folding of a stem-loop RNA structure, and on formation of a triplex structure in a pH-sensitive DNA switch. The results indicate that encapsulation promotes RNA-RNA association, both intermolecular and intramolecular, and also stabilizes tertiary folding, including the docked conformation characteristic of the active hairpin ribozyme, as well as the triplex structure. The effects of encapsulation were sufficient to rescue the activity of folding-deficient mutants of the hairpin ribozyme. Stabilization of multiple modes of nucleic acid folding and interaction thus enhanced the activity of encapsulated nucleic acids. Increased association between RNA molecules might facilitate formation of more complex structures as well as cooperative interactions. These effects could promote the emergence of biological functions in an RNA World, and may have utility in the construction of minimal synthetic cells.

Graphical Abstract

*Lead Contact: ireneachen@ucla.edu.

Author contributions

H.P., S.M. and I.A.C. conceived and designed the study. H.P., A.L., and K.L. conducted experimental work. H.P., S.M. and I.A.C. analyzed the data and drafted the manuscript. All authors commented on the manuscript.

Declaration of interests

The authors declare no competing interests.

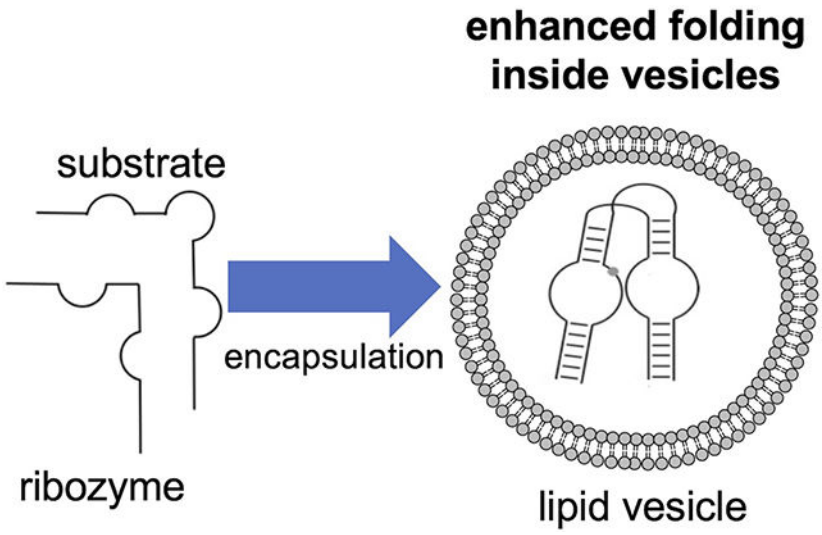

eTOC Blurb

Peng et al. study the effect of vesicle encapsulation on the hairpin ribozyme, a stem-loop RNA and a pH-sensitive DNA switch. They find that encapsulation enhances RNA association and tertiary folding of the nucleic acids. These effects could promote the emergence of biological functions in an RNA world of early life.

Introduction

Encapsulation of nucleic acids, particularly RNA, is a subject of increasing interest in bottom-up synthetic biology. Ribozymes encapsulated inside simple vesicles are an important experimental model of the 'RNA World' of early cells, as encapsulation is essential for creating the physical and genetic unit of the cell.[1–7] In addition, vesicles encapsulating gene circuits are a potential platform for artificial cells.[8–11] Interactions between RNA and vesicles can result in a rich range of emergent behaviors, including vesicle growth driven osmotically by RNA,[12] control of ribozyme reactions by oligonucleotides during vesicle growth,[13] and physical stabilization of fatty acid vesicles by nucleobases.[14] Encapsulation itself has been observed to increase binding activity of an RNA aptamer,[15] and to accelerate evolutionary adaptation[16] during *in vitro* selection of ribozymes by increasing the variance of fitness. However, the structural basis for these changes in activity and fitness is not well-understood.

RNA function depends on structure,[17] which is critically influenced by the chemical and biophysical environment. The cellular environment is understood to have important effects in modern cells, through chemical interactions as well as excluded volume effects. Molecular crowding has been shown to improve the activity of the hairpin ribozyme by increasing the rate of docking,[18] increase activity of an HDV-like ribozyme under relatively low Mg^{2+} concentrations[19], increase activity of the hammerhead ribozyme, [20,21] and to increase activity of a group I ribozyme, compensating for low Mg^{2+} concentrations.[22] Molecular crowding agents appear to stabilize compact folds, as demonstrated for a group

II intron ribozyme[23] and a group I ribozyme[24,25], to the extent that molecular crowding rescues the activity of group I ribozyme mutants.[26] Similarly, the activity of a bimolecular version of RNase P ribozymes is improved by crowding agents, as constructs with no detectable activity can be activated by addition of polyethylene glycol.[27] In an aqueous two-phase system, partitioning of RNA creates a concentrated and crowded phase in which ribozyme activity is substantially enhanced.[28] Confinement of a macromolecule inside a membrane vesicle creates an excluded volume effect similar to crowding. On theoretical grounds, like crowding, encapsulation is predicted to favor compact structures, shifting the conformational equilibrium toward folded, functional structures[29].

Here we probed the effect of encapsulation on nucleic acid association, structure, and function, using three model systems: the hairpin ribozyme, an RNA stem-loop, and a pH-sensitive DNA switch. The hairpin ribozyme is a small self-cleaving ribozyme derived from the Tobacco Ringspot Virus satellite RNA,[30,31] whose mechanism and folding pathway is well-studied (Figure 1A). The naturally self-cleaving hairpin ribozyme structure can be engineered for cleavage in *trans,* such that suitable RNA substrates are cleaved in a multiple-turnover reaction. Cleavage is reversible, and both cleavage and ligation reactions proceed via the same reaction path in opposite directions.[32] The minimal catalytic structure of the hairpin ribozyme consists of four Watson-Crick base-paired helices separated by two loops (A and B). A key element of the catalytic complex is a ‘docked’ intermediate, in which loops A and B are brought into close contact.[33,34] Upon docking, the catalytic center is created and a transesterification reaction occurs, in which the O2′ at the cleavage site attacks the adjacent phosphodiester linkage by an S_N2-like mechanism, with departure of the O5′ and formation of a cyclic 2′,3′-phosphate (Figure 1).[35] A stably docked intermediate is essential for ligation activity, but self-cleavage can occur, albeit at a reduced rate, even for mutants in which the ribozyme is only transiently docked.[36,37] Therefore, formation of the docked intermediate affects reactivity. Docking has been monitored in FRET assays by labeling the two stems with appropriate donor and acceptor dyes.[33,38,39] When conducted *in trans* under multiple-turnover conditions, the hairpin ribozyme reaction follows Michaelis-Menten kinetics, allowing the effect of lipids and encapsulation to be separately evaluated for catalytic steps or substrate association. To probe the effect of encapsulation on secondary structure formation alone, an RNA stem-loop was used as a simple two-state folding system. Then, to probe how encapsulation affects formation of noncanonical base pairing, intramolecular triplex formation in a DNA ‘switch’ was studied.

Vesicles made from fatty acids are a model for primitive or artificial cells, as they allow for diffusion of nutrients and ions and exhibit a variety of dynamic behaviors on a laboratory time scale, including sustainable growth and division cycles coupled with encapsulated RNA replication.[40–43] Although fatty acid vesicles are very sensitive to the presence of divalent cations, addition of phospholipids to these vesicles results in greater stability, enabling the study of ribozymes that have relatively high Mg^{2+} requirements.[44] While lipids may exhibit effects on RNA due to chemical interactions in addition to excluded volume effects, comparison of encapsulated RNA to non-encapsulated RNA, exposed to empty vesicles, controls for chemical interactions and can thereby isolate the effect of confinement.[15] We find that encapsulation stabilizes multiple modes of nucleic acid folding,

including intermolecular RNA-RNA association, secondary structure formation, and tertiary interactions.

Results

Multiple-turnover kinetics of the hairpin ribozyme: encapsulation preserves and enhances cleavage activity.

Vesicles were prepared from a 1:1 mixture of oleic acid and POPC (1-palmitoyl-2-oleoyl-glycero-3-phosphocholine), a composition known to be stable in the presence of 10 mM Mg^{2+}.[44] Large unilamellar vesicles were prepared by extrusion to 100 nm diameter (Figure S1a). We determined the cleavage activity of the hairpin ribozyme in the absence of vesicles (i.e., in buffer without lipids), exposed to empty vesicles but not encapsulated ("OutV") and encapsulated inside vesicles ("InV"). Since the activity of the hairpin ribozyme is dependent on Mg^{2+} concentration, [Mg^{2+}] was varied from 5 to 10 mM. The lipid concentration was varied from 10 to 50 mM to test the dependence of activity on [lipid]. To determine Michaelis-Menten rate constants in a multiple-turnover reaction with excess substrate, the ribozyme:substrate ratio was varied from 1:5 to 1:100.

We determined the Michaelis constant (K_m) and catalytic rate constant (k_{cat}) of the hairpin ribozyme under the different conditions. Cleavage of substrate RNA **1** (Table S1) by the ribozyme releases a 6-nucleotide, dye-labeled product (Figure 2A). Product formation was followed over time by denaturing gel electrophoresis (Figure 3) and fit to a Michaelis-Menten kinetic model following a previously described procedure (STAR Methods, Figure S1–3).[45]

K_m and k_{cat} for encapsulated ribozymes (InV) were compared to the values for ribozymes that were exposed to empty vesicles (OutV) or in lipid-free solution. Exposure to empty vesicles, i.e., having ribozymes on the outside of vesicles, caused increased K_m (Figure 4, A–C), consistent with prior observations that lipids act as a denaturant.[46] Indeed, exposure to high concentrations of lipid caused loss of detectable activity in the OutV condition (Figure S4). However, encapsulation inside vesicles (InV) yields lower K_m at the same lipid concentrations, and preserved activity at concentrations that had resulted in no detectable activity in the OutV condition. In addition, at low [Mg^{2+}] (5 mM; Figure 4A), encapsulation resulted in a significantly lower K_m compared to lipid-free solution, indicating that encapsulation can not only prevent loss of binding but also improve activity. While increasing lipid concentration caused increased K_m in the OutV condition, encapsulation (InV) rendered the K_m insensitive to lipid concentration over the tested range.

A similar pattern was observed for the rate constant k_{cat} and catalytic efficiency k_{cat}/K_m (Figure 4, D–F and G–I, respectively). Exposure to increasing lipid concentration (OutV) decreased k_{cat} and k_{cat}/K_m with activity being undetectable at high lipid concentrations (Figure S4I), again consistent with denaturation upon lipid exposure. However, when encapsulated (InV), k_{cat} and k_{cat}/K_m remained high and were not affected by lipid concentration, tolerating lipid concentrations that would otherwise result in no activity (STAR Methods).

Notably, encapsulation was observed to prevent inactivation of the hairpin ribozyme at higher lipid concentrations (Figure 4). At low [Mg^{2+}] (5 mM), exposure to empty vesicles with ≥30 mM lipid caused inactivation of the ribozyme (i.e., undetectable activity in the OutV condition), but encapsulated ribozymes were active at all lipid concentrations tested (STAR Methods). Overall, encapsulation improved K_m, maintained catalytic activity and efficiency at increasing lipid concentrations, and rescued the ribozymes from lipid-based inactivation.

Single-turnover kinetics of hairpin ribozyme cleavage: the catalytic step is insensitive to lipids.

The k_{cat} determined from the multiple-turnover cleavage reactions encompasses several microscopic steps, including association, docking, cleavage, undocking, and product dissociation[34] (Figure 1B). To probe how lipids and encapsulation affect docking and cleavage independent of substrate association and product dissociation, we performed single-turnover cleavage reactions with the hairpin ribozyme and substrate RNA **1** and assayed them by gel electrophoresis, with a 10-fold excess of ribozyme over substrate (Figure 3A, Figure S4G,H,J). In the single-turnover case, the observed rate constant, $k_{obs,cleav}$, reflects the docking and cleavage steps, of which docking may be rate-limiting.[34] The findings (STAR Methods) mirror the trends observed with k_{cat} in the multiple-turnover condition. Thus, the presence of empty vesicles perturbs the catalytic steps somewhat, but the main inactivating effect of empty vesicles, seen prominently in the multiple-turnover scenario, occurs primarily at non-catalytic steps (e.g., substrate association and dissociation).

Encapsulation promotes docking of the hairpin ribozyme.

Since confinement in a small volume is expected to stabilize compact structures relative to unfolded structures,[15,29] we hypothesized that encapsulation may cause the observed effects on k_{cat} of the hairpin ribozyme through stabilization of the ‘docked’ conformation, which contains an essential tertiary contact on the reaction pathway. Formation of the docked conformation was measured using fluorescence resonance energy transfer (FRET; Figure 2B), in the following conditions: in the absence of vesicles, exposed to empty vesicles (OutV), or encapsulated inside vesicles (InV). The ribozyme was labeled with donor and acceptor dyes and incubated with a non-cleavable modified RNA **5** as substrate (Figure S5A–D; Table S1). For the wild-type hairpin ribozyme (RNA **2**; Table S1), the largest FRET signal was observed in the absence of vesicles, consistent with the observation that k_{cat} is also highest under this condition (Figure 5B, Figure S5E–K, Table S2). Exposure of the ribozyme to empty vesicles reduced both the rate of docking and the overall FRET signal, indicating less docking as the amount of lipid increased, down to 44% signal and to 38% rate (at 30 mM lipid) compared to the lipid-free solution. However, when the ribozyme was encapsulated inside vesicles at the same lipid concentrations, the FRET signal equilibrated at ~79%, with the docking rate at ~70%, compared to the lipid-free solution. This indicates a shift toward the docked state when the ribozyme is encapsulated compared to the OutV condition. Furthermore, the FRET signal was insensitive to increasing lipid concentration when the ribozyme was encapsulated, in contrast to the OutV condition, where the FRET signal and docking rate decreased as the [lipid] increased. The shift toward the docked state and the insensitivity of the FRET signal to [lipid] mirror the trends seen

with cleavage activity of the ribozyme, supporting the idea that encapsulation promotes activity by favoring a compact tertiary conformation along the reaction pathway.

Rescue of docking in folding-deficient ribozyme mutants via encapsulation.

Since encapsulation was observed to favor the docked state, we tested whether encapsulation could rescue known folding-deficient mutants (C25U and A10G,[36,37] corresponding to RNA **3** and **4** respectively; Table S1; Figure S5A–D). These mutants normally exhibit no detectable docking in solution. The ribozymes were annealed with non-cleavable substrate RNA **5** to study docking by FRET. Indeed, these mutants do not show detectable FRET signals in the absence of vesicles or when exposed to empty vesicles (Figure 5C, Figure S5L–Z8). However, encapsulation of these mutants results in significant FRET signals, with mutant C25U recovering to ~36% and mutant A10G recovering to ~53% of the wild-type docking signal amplitude (and to ~23% and 33%, respectively, for docking rate) (Table S2). In the case of mutant C25U, activity is known to be partly rescued by compensatory mutation G+1A in the substrate.[36] When mutant C25U was assayed with the compensatory substrate (RNA **6**, Table S1; Figure S5A–D), docking was still not detectable in buffer (without lipids) or when exposed to empty vesicles (Figure S5Z2–Z8). However, encapsulation of the C25U/G+1A complex does result in higher FRET signals than those observed with C25U and substrate **5** (recovering to ~56% of both wild-type signal amplitude and docking rate), consistent with the known effect of G+1A. For encapsulated reactions, the level of FRET signal was insensitive to the lipid concentration, consistent with the earlier observations of kinetics. These results indicate that encapsulation restores and improves docking for these mutants.

Cleavage activity of the mutants with vesicles.

Given the improvements in docking observed for encapsulation, we then measured the catalytic activities of the folding-deficient mutants in the lipid-free buffer, encapsulated inside vesicles, or exposed to empty vesicles. These mutants are known to be capable of cleavage despite their folding defects.[36,37] Both mutants, and the C25U/G+1A complex (using substrate RNA **7**), showed higher cleavage activity when encapsulated inside vesicles compared to lipid-free buffer or exposure to empty vesicles (Figure 6A–C, Figure S6A–C), with the observed rates being approximately doubled when encapsulated compared to lipid-free buffer (Table S3, Section 1). This observation indicates that the restoration of docking by encapsulation, as measured by FRET, corresponded to greater cleavage activity. Encapsulation increased cleavage activity over a lipid-free solution, indicating an advantage beyond overcoming the denaturing effect of lipids. As with the wild-type, the beneficial effects of encapsulation were weaker in larger vesicles that had been extruded through 200 nm pores (Figure S6G–K, Table S3, Section 3).

Ligation activity of folding-deficient mutants with vesicles.

In the known folding pathway of the hairpin ribozyme, cleavage or ligation can occur only from the docked state.[34] For the cleavage reaction, the cleavage step can take place, and the fragments can dissociate upon undocking, even if the ribozyme is only transiently docked (undetectable by FRET). However, ligation is apparently more demanding, requiring

a kinetically stable tertiary structure.[37] The folding-deficient mutants normally show no detectable ligation activity, and thus, ligation represents a stronger test of activity compared to cleavage. We studied the ligation activity of mutants A10G and C25U/G+1A in comparison to the wild-type hairpin ribozyme in lipid-free solution as well as the InV and OutV conditions. The reaction (Figure 2C) was monitored by gel electrophoresis using fluorescent substrate RNA **9** (wild-type or A10G) or **10** (C25U/G+1A). As expected, the wild-type ribozyme showed ligation activity in all conditions (Figure 6D and Figure S6D–F, Table S4, Section 1). As observed with the cleavage reaction, ligation activity decreased with increasing lipid concentration when the wild-type ribozyme was exposed to empty vesicles, and encapsulation resulted in improved activity that was not affected by the lipid concentration.

Consistent with the FRET studies, the folding-deficient mutants showed no ligation activity in the absence of vesicles, and also no activity when exposed to empty vesicles. However, ligation activity was restored by encapsulation, consistent with the observation of restored docking in the FRET study. The C25U/G+1A complex was more active in the ligation reaction than the mutant A10G, consistent with the faster docking of C25U/G+1A, as indicated by the FRET study. The detection of ligation activity of the mutants confirmed that encapsulation substantially stabilized the docked conformation, to the extent that ligation was detectable. As seen for the cleavage reaction, the encapsulation effect for ligation was weaker in larger vesicles that had been extruded through 200 nm pores (Figure S6G–K, Table S4, Section 2).

Encapsulation of an RNA stem-loop structure.

Studies with the hairpin ribozyme suggested that encapsulation may affect both secondary (e.g., demonstrated by decreased K_m) and tertiary structure formation (e.g., docking). To directly test the effect of encapsulation on secondary structure formation alone, we studied the melting point of a stem-loop RNA (RNA **11**, Table S1).[47] Formation of secondary structure was followed by FRET (Figure 7A). Exposure to vesicles destabilized the stem-loop structure, with the melting temperature T_m being decreased by around 1.1, 4.4 and 5°C at lipid concentrations of 10, 20, and 30 mM respectively (Figure 7B, Figure S7A–G, Table S4, Section 3). However, the T_m increased by around 2°C when the stem-loop RNA was encapsulated inside vesicles. The results indicate that encapsulation can stabilize base-pairing interactions between strands of nucleic acids.

Encapsulation of a DNA switch.

To test the generality of the observed promotion of tertiary contacts, we studied the folding of a pH-sensitive DNA switch. In this switch, a DNA triplex is formed at low pH, and high pH triggers the release of a single-stranded region from a duplex.[48] The release of the single-stranded DNA could be used to activate downstream events.[49,50] Here, the DNA was labeled with a fluorophore and quencher, such that the fluorescence is quenched when the triplex structure is formed, and fluorescence is recovered when the single-stranded region is released. The switch is characterized by its pK_a, which can be determined as the inflection point of the fluorescence curve over a pH range. In lipid-free solution, the pK_a was observed to be 8.69 ± 0.16. Consistent with our general observation that exposure

to vesicles destabilizes folding, we found that exposure to empty vesicles destabilized the triplex relative to the duplex (Figure 7C,D; Figure S7H–L), lowering the pK_a by ~ 0.5 pH units, to 8.27 ± 0.16 (10 mM lipid) or 8.11 ± 0.15 (20 mM lipid). However, encapsulation inside vesicles stabilized the triplex beyond the pK_a of the switch in lipid-free solution, raising the p*K*a by around 1.0 unit (or by around 1.5 units compared to the switch exposed to empty vesicles), to 9.67 ± 0.17 (10 mM lipid) or 9.68 ± 0.13 (20 mM lipid). Thus, encapsulation significantly shifted the equilibrium of the DNA switch toward triplex formation, consistent with favoring of the compacted structure.

Discussion

Prior studies indicated that encapsulation could increase aptamer and ribozyme activity, but the structural basis of this effect was unknown.[15,16] Here, we determined several effects of encapsulation on RNA and DNA structure and function. First, encapsulation can stabilize RNA structures. This was observed by FRET in the case of the hairpin ribozyme, in which encapsulation promoted docking as well as catalytic activity (STAR Methods). The possibility of encapsulation promoting RNA-RNA structures was further tested in an intramolecular context using an RNA sequence designed to fold into a stem-loop structure. The stem-loop RNA exhibited a higher melting temperature when encapsulated compared to both lipid-free solution and exposure to empty vesicles, indicating a stabilized secondary structure. This presents an interesting comparison with the effects observed in the presence of molecular crowding agents [21,24,51–58] (STAR Methods) and indicates that both intramolecular and intermolecular RNA-RNA base-pairing associations were promoted by encapsulation.

A striking effect of encapsulation was the preservation of multiple-turnover catalytic activity of the hairpin ribozyme when subject to high concentrations of lipids that would otherwise inactivate the ribozyme. The presence of empty vesicles decreased k_{cat}, $k_{obs,cleav}$, docking, and substrate association, leading to ribozyme inactivation in the multiple-turnover condition at high [lipid]. However, all of these steps mostly recovered when ribozymes were encapsulated. Indeed, encapsulation rendered the ribozymes essentially insensitive to lipid-based denaturation, as shown by measurements of docking, K_m, k_{cat}, and $k_{obs,cleav}$. Thus, in addition to promoting secondary structures, encapsulation promoted a tertiary interaction along the reaction pathway, contributing to the observed preservation of catalytic activity under otherwise denaturing conditions (STAR Methods).

The ligation activity of the hairpin ribozyme represents a relatively stringent test of structure formation, particularly docking, since, in contrast to cleavage activity, the docked state must be substantially populated in order for ligation to occur.[36,37] This has been shown in particular for hairpin ribozyme constructs where the essential interdomain GC base pair (G+1C25) was replaced by either an AU pair or a GU wobble pair, as well as for a mutant where the essential adenosine at position 10, involved in formation/stabilization of the active site, was replaced by a guanosine (A10G). These mutants still could cleave their respective substrates, but did not show detectable docking or ligation.[36,37] However, as shown here, encapsulation of these folding- and ligation-deficient mutants restored both detectable docking and ligation activity (see STAR Methods for a discussion of cleavage in

the mutants). Taken together, encapsulation was shown to support activity of the hairpin ribozyme by strengthening important structural interactions. Similar effects have been observed through molecular crowding,[18] where the docking rate of the hairpin ribozyme (10 mM Mg^{2+}, as used in the present FRET study) was observed to increase from 0 to 25% PEG-8000, up to a 7-fold increase in rate. In the present study, encapsulation gave an increase of docking rate and amount by ~1.8-fold compared to the OutV condition; a quantitatively similar increase was observed with approximately 10% PEG-8000 in the prior study. A similar effect was also observed for hairpin ribozymes under compression, wherein particular favorable interactions between the reaction site and neighboring nucleobases were suggested to be stabilized and to accelerate the cleavage step as a consequence.[59]

To test whether encapsulation would stabilize other tertiary interactions, we tested a pH-sensitive DNA switch, in which a triplex interaction forms at low pH, and releases a single strand to adopt the duplex form at high pH. Considering the triplex-duplex equilibrium as an acid-base reaction, encapsulation shifted the pK_a of the triplex by ~1.0 units compared to DNA in lipid-free solution (or by ~1.5 units compared to the lipid-exposed DNA). This shift translates into a free energy stabilization of −1.4 kcal/mol compared to DNA in lipid-free solution (or −2.0 kcal/mol compared to lipid-exposed DNA). For context, these free energy stabilization values are similar in magnitude to the stabilization engendered by an additional base pair.[60] Interestingly, molecular crowders can also stabilize triplex formation,[61] consistent with the idea that vesicle confinement acts as an excluded volume effect.[15,29] The results showing decreased effect in larger vesicles also supports the interpretation that the confined volume causes the observed effects for the systems studied here. Encapsulation thus stabilized tertiary contacts in nucleic acids, as observed for both docking in the hairpin ribozyme as well as triplex formation in the DNA switch.

The observation that encapsulation stabilizes nucleic acid structures, and rescues inactive mutants of the hairpin ribozyme, has implications for the emergence and evolution of ribozymes in an RNA world. This stabilization would be particularly important in a prebiotic milieu containing a high concentration of lipids, which denature non-encapsulated RNA. The presence of lipids represents a double-edged sword for ribozymes: lipids increase the fitness of ribozymes that happen to become encapsulated, but they simultaneously depress, potentially severely, the fitness of ribozymes that are not encapsulated.

Given the general nature of the confinement effect in favoring compact (i.e., folded) structures for a variety of sequences, the frequency of sequences exhibiting an activity would increase if encapsulated, implying greater discoverability of such sequences from a random pool. In addition, as has been suggested for molecular crowding,[26] encapsulation would increase the mutational tolerance of a ribozyme. Tolerance to mutations would be a critical property, since replication error rates were likely high during the early stages of life. In particular, mutational tolerance would help avoid an ‘error catastrophe’ by reducing the amount of information that must be replicated faithfully.[62,63] Furthermore, stabilization of intermolecular RNA-RNA interactions might promote cooperative phenotypes, such as a system of mutually self-replicating ligases[64] or an autocatalytic set of recombinases[65], or formation of an active structure from smaller RNA subunits[66–68]. Thus, the physical

confinement provided by encapsulation could facilitate the emergence of more complex catalytic activities during the origin of life.

STAR ★METHODS

RESOURCE AVAILABILITY

Lead contact

- Further information and requests for resources and reagents should be directed to and will be fulfilled by the lead contact, Irene Chen (ireneachen@ucla.edu).

Materials availability

- This study did not generate new unique reagents.

Data and code availability

- All data reported in this paper will be shared by the lead contact upon request.
- This paper does not report original code.
- Any additional information required to reanalyze the data reported in this paper is available from the lead contact upon request.

METHOD DETAILS

Preparation of phospholipid/oleic acid vesicles—The phospholipid/oleic acid vesicles were prepared according to previous methodology.[69] Briefly, 2.4 μL oleic acid in 200 μL methanol and 228 μL POPC in chloroform (25 mg/mL) were mixed well by vortexing and dried by rotary evaporation onto a round-bottom flask. One equivalent of 1 M KOH (7.6 μL) was added and the phospholipid/oleic acid solution was resuspended in 10 mM Tris–HCl (pH 7.5) buffer. The vesicles were prepared by extrusion through 100 nm (or 200 nm, when noted) polycarbonate membrane filters (Whatman) using a Mini-Extruder (Avanti Polar Lipids, Alabaster, AL). The vesicle solutions were concentrated by ultrafiltration to approximately 150 μL with an Amicon Ultra-4 10 000 filter. Assuming negligible loss of lipid, the lipid concentration after ultrafiltration is 100 mM (concentration of POPC + concentration of oleic acid). The concentration of oleic acid was verified by the ADIFAB assay (FFA Science, United States)[69], which measured 47 ± 3 mM fatty acid in the stock solution. Given the 1:1 ratio of oleic acid to phospholipid, the total measured lipid concentration in the stock was ~94 mM, which was comparable with the expected concentration of 100 mM.

Dynamic Light Scattering (DLS) measurement—Vesicle size was measured by DLS using the Zetasizer Nano ZSP (Malvern Instruments, UK). Photons were collected at 173° scattering angle and the scattering intensity data were processed using the instrumental software to determine the hydrodynamic size of the vesicles.

Encapsulation of RNA or DNA—The ribozyme and substrate RNA of designed ratios were mixed with buffer so as to obtain a final concentration of ~0.43-47 μM RNA in 10 mM Tris–HCl (pH 7.5) buffer. This solution was added to the phospholipid/oleic acid

micellar stock to prepare vesicles encapsulating RNA. For experiments on encapsulation of the ribozyme and substrate RNA inside vesicles, the unencapsulated RNA was removed by size exclusion chromatography (SEC) with Sepharose 4B resin (Figure S1b). Vesicles were extruded and purified from unencapsulated (free) RNAs using a Sepharose 4B size exclusion column (SEC) with a mobile phase of 10 mM Tris–HCl (pH 7.5) buffer. The vesicle solutions were concentrated by ultrafiltration to the desired lipid concentration (verified by ADIFAB assay as described above) with an Amicon Ultra-4 10 000 filter. The DNA switch and hairpin RNA structures were encapsulated in a similar way described above. The fluorescence signals of the collected products from SEC were measured on a TEC AN infinite 200 Pro plate reader (TEC AN, Switzerland).

Cleavage experiments—For cleavage experiments without vesicles, the solution of the ribozyme and the 5′- fluorescein-labelled substrate strands (RNA **1** or **7**) in 10 mM Tris–HCl (pH 7.5) were incubated at 90°C for 1 min followed by cooling to 37°C for 15 min. The cleavage reactions were started by adding an appropriate volume of the $MgCl_2$ stock solution to the reaction mixture by brief pipetting at $t = 0$. In a typical cleavage experiment, final concentrations were 10 nM ribozyme, 50, 100, 200, 400 or 1000 nM (multiple turnover), or 1 nM (single turnover) substrate and 5 (7 or 10) mM $MgCl_2$ in a final volume of 20 μL. Aliquots (1.5 μL) of the reaction mixture were removed at time intervals and the reaction quenched by addition to 3 μL of stop mix (7 M urea, 50 mM EDTA). The samples were analyzed by 12% denaturing polyacrylamide gel electrophoresis and imaged using Amersham Typhoon Gel Imager (GE, USA). For cleavage experiments of RNA exposed to empty vesicles, the lipid concentrations were adjusted to 10, 20, 30, 40 and 50 mM. The aliquots of the reaction mixture were added to 3 μL of stop mix (7 M urea, 50 mM EDTA) with 0.6% Triton X-100 to rapture the vesicle for 30 min at room temperature. For experiments using non-extraded vesicles. vesicles were prepared in the same manner without the extrusion step, lipid concentrations were adjusted to match experiments with extruded vesicles, and cleavage experiments were performed as described above. For cleavage experiments of RNA encapsulated in vesicles, the lipid concentrations were 10, 20 and 50 mM. Vesicles were extruded to 100 nm unless otherwise noted, and experiments were performed following the same procedure regardless of vesicle extrusion size. At least three independent replicate data sets were collected.

Ligation experiments—The wild-type hairpin ribozyme and mutants A10G and C25U/G+1A (see STAR Methods for sequences) were used for the ligation experiments. In general, ligation-competent ribozyme-substrate complex is prepared by annealing the ribozyme strand with a cleavage substrate and conducting the cleavage reaction. Dissociation of the smaller 3’ cleavage product results in the ribozyme strand in complex with the 5’ substrate strand. Then, addition of a fluorescently labeled 3’ substrate strand and higher $[Mg^{2+}]$ allows assessment of ligation activity (Figure 2C). For ligation experiments without vesicles, 20 μL of the ribozyme (200 nM) and the unlabeled substrate (100 nM; RNA 8) strands in 10 mM Tris–HCl (pH 7.5) were incubated at 90°C for 1 min followed by cooling to 37°C for 15 min. Then an appropriate volume of the $MgCl_2$ stock solution was added to the reaction mixture by brief pipetting for the final Mg^{2+} concentration of 7 mM. The sample was incubated at 37°C for 1 h. Then the appropriate amount of 5’-fluorescein-

labelled ligation substrate (RNA **9** or **10**; see Table S1) stock solution and $MgCl_2$ stock solution were added to the reaction mixture to make the final ratio of ribozyme:ligation substrate equal to 1:1 and the Mg^{2+} concentration equal to 10 mM; the time of this addition was defined as time $t = 0$. Aliquots (1.5 μL) of the reaction mixture were removed after adding the ligation substrate, at particular time intervals, and the reaction quenched by addition to 8.5 μL of stop mix (7 M urea, 50 mM EDTA). The samples were analyzed by 12% denaturing polyacrylamide gel electrophoresis and imaged using an Amersham Typhoon Gel Imager (GE, USA).

For ligation experiments of RNA exposed to empty vesicles, the reaction procedure is identical to that mentioned above but with the lipid concentrations included in the buffer equal to 10, 20 or 30 mM. The aliquots of the reaction mixture were quenched by addition of 8.5 μL of stop mix (7 M urea, 50 mM EDTA) with 0.6% Triton X-100 and incubated for 30 min at room temperature to rupture the vesicles.

For ligation experiments of RNA encapsulated in vesicles, the fluorescently labeled ligation substrate could not be added during a second step. Instead, the ribozyme, cleavage substrate and fluorescently labelled ligation substrate were annealed together (incubated at 90°C for 1 min followed by cooling to 37°C for 15 min) and encapsulated in the vesicles as described above. The concentration of Mg^{2+} was brought 7 mM and the reaction was incubated at 37°C for 1 h to prepare the ligation-competent ribozyme complex. The concentration of Mg^{2+} was then brought to 10 mM, defining $t = 0$. Aliquots (1.5 μL) of the reaction mixture were removed at time intervals and the reaction quenched by addition to 8.5 μL of stop mix (7 M urea, 50 mM EDTA) with 0.6% Triton X-100 and incubation for 30 min at room temperature to rupture the vesicles. The lipid concentrations were the same as mentioned above for the reactions exposed to empty vesicles. At least three independent data sets were collected. Ligation experiments using vesicles of different sizes were performed in the same way.

Fluorescence resonance energy transfer (FRET) measurement—The FRET measurement was performed on a Fluoromax 4C (Horiba) with a Peltier-controlled temperature attachment (Model F-3004, Horiba). The wild-type hairpin ribozyme (RNA **2**), mutants A10G (RNA **4**), C25U (RNA **3**), and C25/G+1A (RNA **3** + **6**), and the corresponding non-cleavable substrate (RNA **5** or **6**) (Figure S5a–d; Table S1) were used for FRET measurements. Doubly labeled ribozyme (50 nM; see below for labelling method) and a 20-fold excess of non-cleavable substrate were mixed and pre-incubated in 10 mM Tris-HCl (pH 7.5) at 37 °C for 15 min, before manually adding $MgCl_2$ stock solution (final concentration = 10 mM) to initiate domain docking. Atto 488 was excited at 450 nm. Fluorescence emission was monitored at both 520 nm (for the Atto 488 donor) and 590 nm (for the Atto 565 acceptor), and the ratio $Q = F_{590}/F_{520}$ was calculated as a function of time. This ratio Q was normalized by its initial value Q_0 (i.e., $y = (Q\text{-}Q_0)/Q_0$). The resulting curves were fitted with the exponential function $y = A(1\text{-}e^{-k\text{dock}t})$. Here k_{dock} is the observed docking rate constant and A is the observed relative docking amplitude. For FRET measurement of RNA exposed to empty vesicles, vesicles with the desired lipid concentrations were mixed with the ribozyme and non-cleavable substrate strands and preincubated in 10 mM Tris-HCl (pH 7.5) at 37 °C for 15 min before manually adding

$MgCl_2$ stock solution. For FRET measurement of RNA encapsulated inside vesicles, the ribozyme and non-cleavable substrate were annealed together by heating to 90°C for 1 min, followed by cooling down to 37 °C for 15 min before encapsulation as described above. Then, vesicles containing the ribozyme and non-cleavable substrate strands were preincubated in 10 mM Tris-HCl (pH 7.5) at 37 °C for 15 min, before manually adding $MgCl_2$ stock solution to initiate docking.

Melting transitions of RNA measured by FRET—A stock solution (100 μM) of the FRET-labeled stem-loop RNA **11** was heated to 75 °C for 5 min and slowly cooled down to room temperature to anneal the RNA structure. The fluorescence of the dye-labelled RNA was measured at different temperatures using a Fluoromax 4C (Horiba) with a Peltier-controlled temperature attachment (Model F-3004, Horiba). The fluorescence of the labeled RNA was recorded in 3 °C increments from 10 to 67 °C, with a 10 min incubation at each interval. Fluorescence intensity spectra (excitation at 450 nm, and emission spectrum between 480 and 700 nm) were recorded. Melting curves were fitted in Origin Pro 9 software using the Boltzmann sigmoidal equation $R = R_{min} + (R_{max} - R_{min})/(1 + \exp((T_t - T)/s))$, where R refers to normalized fluorescence intensity ratio of F_{520nm}/ F_{590nm}, and R_{min} and R_{max} are the minimum and maximum values, respectively, T is temperature, T_t is the transition temperature, and s is a fitting parameter. T_t values presented here are an average of three independent experiments.

pH-titration measurements—The pH-titration curves of the pH-sensitive DNA switch (100 nM; STAR Methods) were conducted in a universal citrate/phosphate/borate buffer whose pH was adjusted to the desired value. The solutions of the universal buffer at different pH were prepared according to a previously reported method.[70] Equilibrium fluorescence measurements were obtained using a Fluoromax-4C spectrofluorometer (Horiba) with excitation at 488 nm and acquisition between 540 and 650 nm at 25°C. The normalized fluorescence data F (at 572 nm) was fitted with the following equation: $F= F_0+ (F_m-F_0) \times 10^{-k}/(10^{-k}+10^{-x})$.[48] In this equation, F_0 is the minimum fluorescence signal (triplex state); F_m is the maximum fluorescence signal (duplex state); k is the pH of the inflection point, and x is the pH of the solution.

Synthesis and labelling of RNAs—RNAs (Table S1) were chemically synthesized on a GeneAssembler (Pharmacia) using phenoxyacetyl (PAC) protected β-cyanoethyl-(*N,N*diisopropyl)-phosphoramidites of 5′-*O*-dimethoxytrityl-2′-*O*-tertbutyldimethylsilyl (TBDMS) nucleosides as described previously.[71] RNA sequences A_WT, A_MUT C25U and A_MUT A10G were modified at the 5′-terminus with an amino linker using C6-NH_2 phosphoramidite, and at the 3′-terminus with an alkynyl group using 2′-O-propargyluridine-3′-lcaa on CPG 1000 Å. RNAs Lig_3′-Frag G and Lig_3′-Frag A were modified at the 3′-terminus only with an alkynyl group. All RNAs were purified on 15% denaturing polyacrylamide gels, product-containing bands were cut from the gel, and RNAs were eluted (0.3 M NaOAc, pH 7.1) followed by ethanol precipitation.

Double labelling of A_WT, A_MUT C25U and A_MUT A10G was performed with Atto488 NHS-ester and Atto565-azide (ATTO-TEC) in a one-pot reaction. Atto488 NHS-ester (150 μg) was dissolved in 30 μL dry DMF and added to the RNA (6 nmol) in 50 μL sodium

carbonate buffer (0.2 M, pH 8.5). The reaction was allowed to proceed under shaking for 4 h at 25 °C. Subsequently, the Atto488-labeled RNA was added to 50 μg dry Atto565-azide. A mixture of 50 μl $CuSO_4$(1mM in phosphate buffer 0.1 M, pH 7) and 50 μL tris(3-hydroxypropyltriazolylmethyl) amine (5 mM in phosphate buffer 0.1 M, pH 7) was saturated with argon for 5 min and added to the RNA solution, which was again degassed with argon for 5 min. Thereafter, 65 μL of freshly prepared sodium ascorbate solution (8 mM) was saturated with argon for 10 min and added to the reaction mixture. Finally, 240 μL phosphate buffer (0.1 μM, pH 7) were added to the solution. After incubation for 4 h at 37 °C, the labelled RNA was precipitated from ethanol. 3′-end labelling of Lig_3′-Frag G and Lig_3′-Frag A with 5′-FAM (Jena Biosciences) was carried out according to the suppliers' protocol. All labelled RNAs were purified by RP-HPLC (EC 250/4 Nucleodur 100-5 C18, column volume (cv) = 3.142 mL) using buffer A (0.1 M TEAAc, 5% acetonitrile) and a gradient of buffer B (0.1 M TEAAc, 30% acetonitrile): 10% buffer B for 2 cv, 50% buffer B for 5 cv, 80% buffer B for 25 cv and 100% buffer B for 2 cv, at a flow rate of 0.5 mL/min. The isolated labelled RNAs were desalted by gel filtration and stored at −20 °C until further use.

Preparation of hairpin ribozymes by *in vitro* transcription—Hairpin ribozymes were enzymatically synthesized by *in vitro* transcription from a double-stranded DNA template. To generate the DNA template, a Klenow polymerase fill-in reaction was performed using two primers overlapping at their 3′-ends (STAR Methods). Primers with a final concentration of 2 μM in a reaction volume of 500 μL were mixed with the Klenow buffer (50 mM Tris pH 7.6, 10 mM $MgCl_2$ and 50 mM NaCl) and heated for 2 min at 90 °C. After incubation at 37 °C for 15 min, the reaction was started by addition of dNTPs (0.5 mM) and the Klenow fragment exo– (final concentration 0.05 U μL_{-1}). The reaction was carried out for 30 min at 37 °C. The DNA was ethanol-precipitated and purified on a native polyacrylamide gel, eluted from the gel and desalted by ethanol precipitation. For *in vitro* transcription, DNA (1 μM) in transcription buffer (80 mM HEPES pH 7.5, 22 mM $MgCl_2$, 2 mM spermidine, 40 mM dithiothreitol) was mixed with 2 μM NTPs, and 5 μL of T7 RNA polymerase (1 U μL_{-1}) was added to a final volume of 50 μL. Transcription was perfonned for 2.5 h at 37 °C. The DNA template was degraded by addition of DNase I (2 U) followed by incubation at 37 °C for 30 min. RNA was recovered by ethanol precipitation, purified by 12% denaturing polyacrylamide gel electrophoresis, eluted from the gel and desalted by ethanol precipitation.

Detailed kinetic analysis—For each condition, time-dependent data were fit to a single exponential equation to obtain observed rates (k_{obs}) at each ribozyme:substrate ratio (Figure S1–2), and the Michaelis-Menten constants (K_m and k_{cat}) were determined by Eadie-Hofstee analysis. The cleavage reactions fit the Michaelis–Menten kinetic model well (Figure S3A–F). Rates increased with increasing substrate concentration until saturation, confirming the multiple-turnover nature of the reaction when encapsulated (Figure 3D–F, Table S5, S6, Section 1).

Interestingly, in contrast to K_m, k_{cat} for encapsulated ribozymes was lower than for the ribozyme in lipid-free solution (Figure 4D–F). One interpretation of this finding is that

the internal equilibrium of the hairpin ribozyme reaction may be shifted towards ligation (away from cleavage),[38,72–75] leading to reduction of k_{cat} determined for the cleavage reaction. At the same time, ligation would be expected to become more pronounced (see results for ligation assay below). For k_{cat}/K_m, increased K_m compensated for decreased k_{cat}, such that k_{cat}/K_m of encapsulated ribozymes was similar to that in a lipid-free solution. Thus, encapsulation preserves catalytic activity and efficiency in the presence of otherwise denaturing lipids.

At medium (7 mM) and high (10 mM) [Mg^{2+}], exposure to ≥40 mM or to 50 mM lipid, respectively, caused inactivation, but encapsulation again preserved ribozyme activity at the highest [lipid] tested (50 mM). To determine whether extrusion altered the effect of the lipid vesicles, we compared vesicles with or without extrusion (OutV condition). Ribozyme activity (5 mM Mg^{2+}, 10 mM lipid) in both cases was similar (Figure S3G,H and Table S3, Section 2; compare to Figure 3D–F), indicating that the denaturing effect of lipid exposure (OutV) was not very dependent on vesicle size and shape. To determine whether the confinement volume influenced the effect, we found that the beneficial effects of encapsulation were weaker in larger vesicles that had been extruded through 200 nm pores (Figure S4A–F, Table S6, Sections 2 and 3).

Single-turnover kinetics: As expected, comparison to k_{cat} (Figure 4D) showed that $k_{obs,cleav} > k_{cat}$, indicating that additional steps (undocking, dissociation and association) affect k_{cat} in the multiple-turnover reaction. In the single-turnover reactions at low [lipid], the presence of lipids (both InV and OutV conditions) caused a decrease in $k_{obs,cleav}$ that was quantitatively similar to the drop observed for k_{cat} under the same Mg^{2+} and lipid conditions. Interestingly, in contrast to the multiple-turnover reactions, high lipid concentrations did not completely inactivate the reaction in the OutV condition (compare Figure 5A to Figure 4A,D,G). Nevertheless, $k_{obs,cleav}$ decreased as [lipid] increased in the OutV condition, but not when encapsulated (InV). Similarly, the extent of reaction also dropped significantly as [lipid] increased for the OutV condition, but not the InV condition (Figure S4H).

For the wild-type and mutant ribozymes, exposure to lipids (OutV) causes a roughly two-fold decrease in k_{obs}. In the wild-type ribozyme, encapsulation causes only a small increase in k_{obs} compared to OutV, such that the encapsulated k_{obs} is lower than for the lipid-free environment. In contrast, for the mutants, encapsulation leads to relatively large effect on k_{obs}, such that the encapsulated k_{obs} is greater than that of the lipid-free environment. The wild-type ribozyme shows stable docking in buffer, and encapsulation was observed to have only a minor effect on an already stable docking process by FRET. This was reflected in the k_{obs} values, which are determined with k_{dock} or k_{undock} being the rate-limiting steps for the wild-type. The minor nature of the effect resulted in the overall finding that encapsulation did not fully compensate for the denaturation caused by exposure to the lipids (Figure 5A). So, in the wild-type ribozyme, the docked complex is only slightly affected by being inside the vesicle (as shown by the FRET data), and with docking/undocking rates being rate-limiting, k_{obs} shows only a minor effect.

With respect to the mutants, there is no stable docking observed in the lipid-free environment, and encapsulation causes a sufficiently large effect to observe a stably docked state. For the mutants, in particular for the A10G variant, higher cleavage rates than for the wild-type have been observed in vitro[37], and it has been suggested that fast docking/undocking steps lead to a transiently docked complex, sufficient for cleavage to take place, such that docking/undocking steps are no longer rate-limiting. However, our FRET data shows that encapsulation leads to a detectable, stably docked complex, and therefore docking/undocking may be rate-limiting again. The large effect of encapsulation on docking is thus consistent with the observed relatively large increase in k_{obs}, which results in the encapsulated k_{obs} being greater than the lipid-free k_{obs}.

Although the FRET constructs probe an effectively intramolecular interaction, while the cleavage experiments probe an intermolecular reaction, the size of the effect of encapsulation on docking can be compared to the size of effect on cleavage kinetics. In the FRET assay, encapsulation results in a ~1.8-fold increase in both docking rate and amount. Docking is expected to affect both K_m and k_{cat}. In the multiple-turnover reaction performed at the same conditions as the FRET studies (10 mM Mg^{2+}, 30 mM lipid), encapsulation causes the K_m to decrease by approximately 2.5-fold (comparing the InV and OutV conditions), and causes the k_{cat} to increase by ~1.4-fold (comparing InV and OutV). Although the FRET constructs and cleavage constructs are different, the similarity of the magnitudes of these effects suggests that encapsulation effects on docking may be sufficient to explain most of the effect on K_m and k_{cat} of the multiple-turnover reaction. Encapsulation might cause other effects as well, such as changes in effective concentration or alterations in pK_a of catalytically involved residues, but these do not appear necessary to explain the overall effect in this case. The difference in K_m between encapsulated ribozymes vs. ribozymes in lipid-free solution decreased as Mg^{2+} concentration increased, indicating that encapsulation could compensate for low Mg^{2+} with respect to K_m. However, changes in K_m could also reflect changes in k_{cat} ($K_m = (k_{-1} + k_{cat})/k_1$).

DNA primer information—The following primers were used to synthesize DNA templates for *in vitro* transcription preparing hairpin RNA ribozymes. The underlined sequences are overlapping, and the mutant bases are marked in bold.

Wild-type hairpin ribozyme: Forward primer: 5′-TAA TAC GAC TCA CTA TAG GGA GAA AGA GAG AAG TGA ACC AGA GAA A-3′

Reverse primer: 5′-TAC CAG GTA ATA TAC CAC AAC GTG TGT TTC TCT GGT TCA CTT CTC T-3′

Mutant C25U: Forward primer: 5′-TAA TAC GAC TCA CTA TAG GGA GAA AGA GAG AAG TGA ACC AGA GAA A-3′

Reverse primer: 5′-TAC CAG GTA ATA TAC CAC AAC GTG T**A**T TTC TCT GGT TCA CTT CTC T-3′

Mutant A10G: Forward primer: 5′-TAA TAC GAC TCA CTA TAG GGA GAA AGA GAG AGG TGA ACC AGA GAA A-3′

Reverse primer: 5′-TAC CAG GTA ATA TAC CAC AAC GTG TGT TTC TCT GGT TCA CTT CTC T-3′

Triplex DNA switch: The triplex pH-triggered DNA switch is labelled with BHQ-2 (Black hole quencher 2) at position 13 and with Alexa Fluor 546 (AF546) at the 3′end (synthesized by IDT). The sequence of the DNA switch is the following: 5′-AAGAA-AAGAA-TTT(BHQ-2)A-TTCTT-TTCTT-CTTTG-TTCTT-TTCTT (AF546)-3′

Comparison with crowding agents—In the case of an RNA stem-loop structure studied in the presence a variety of crowding agents[51], addition of PEG resulted in increased T_m, by up to 13.4 °C, with the effect size depending on the PEG molecular weight. On the other hand, chemical interactions with the crowding agent can be significant as well; in one study, addition of ethylene glycol and low molecular weight PEG were found to decrease the T_m of DNA duplexes[55] by up to 16 °C, depending on the DNA length and PEG size. In the present study, encapsulation caused a 2-7 °C increase in T_m (depending on the lipid concentration of the OutV comparison), roughly equivalent to addition of 30% PEG-400 or PEG-6000 in the prior study[51] of an RNA stem-loop.

Lipid-based inactivation—In this work, we demonstrated that vesicle encapsulation stabilizes both secondary and tertiary structure elements, as well as intermolecular base-pairing, and thus can impact the activity of functional nucleic acids. These studies also give insight into the phenomenon of lipid-based inactivation, namely that exposure to empty vesicles causes a decrease of activity, or at high concentrations, elimination of activity. This effect is due to exposure to vesicles, rather than to exposure to micelles or molecular lipid, since the denaturing effect increases at concentrations much higher than the critical aggregation concentration (cac) (i.e., upon addition of vesicles at constant micelle and molecular lipid concentration). The concentration of non-vesicular oleic acid (OA) in a 1:1 POPC/OA system was measured to be 3.5 μM, an estimate of the cac[44]; lipid concentrations used in these experiments were several orders of magnitude larger than the cac. The encapsulation effect may be measured against the OutV condition in order to isolate the confinement effect, controlling for the effect of chemical exposure to the lipid[15]. The OutV condition may exclude a small fraction of volume (<10% for up to 30 mM lipid; see Ref.[15] for calculation), but a possible excluded volume effect was apparently not large enough to counter the denaturing effect in these experiments.

QUANTIFICATION AND STATISTICAL ANALYSIS

All statistics were performed in OriginPro 2015 (OriginLab). All values are shown as mean ± standard error of the mean (SEM), as specified in the corresponding figure and table legends.

Supplementary Material

Refer to Web version on PubMed Central for supplementary material.

Acknowledgements

The authors thank James Carothers and Matthew Lakin for advice regarding the DNA switch, Ranajay Saha for advice on encapsulation, and Ulrich Gerland for discussions about energetics. Funding from the Simons Foundation Collaboration on the Origin of Life (Grant 290356FY18), National Science Foundation (Grant 1935087), National Institute of General Medical Sciences (Grant DP2GM123457), Camille Dreyfus Teacher-Scholar Program, and Deutsche Forschungsgemeinschaft (DFG_MU1396/19) is acknowledged.

References

1. Pressman A, Blanco C, and Chen Irene A. (2015). The RNA World as a Model System to Study the Origin of Life. Current Biology 25, R953–R963. 10.1016/j.cub.2015.06.016. [PubMed: 26439358]
2. Saha R, Pohorille A, and Chen IA (2014). Molecular Crowding and Early Evolution. Origins of Life and Evolution of Biospheres 44, 319–324. 10.1007/s11084-014-9392-3.
3. Ichihashi N, and Yomo T (2014). Positive roles of compartmentalization in internal reactions. Current Opinion in Chemical Biology 22, 12–17. 10.1016/j.cbpa.2014.06.011. [PubMed: 25032508]
4. Koonin EV (2012). RNA Worlds: From Life's Origins to Diversity in Gene Regulation edited by Atkins John F., Gesteland Raymond F, and Cech Thomas R.. The Quarterly Review of Biology 87, 66–66. 10.1086/663891.
5. Szostak JW, Bartel DP, and Luisi PL (2001). Synthesizing life. Nature 409, 387–390. 10.1038/35053176. [PubMed: 11201752]
6. Bansho Y, Furubayashi T, Ichihashi N, and Yomo T (2016). Host–parasite oscillation dynamics and evolution in a compartmentalized RNA replication system. Proceedings of the National Academy of Sciences 113, 4045–4050. 10.1073/pnas.1524404113.
7. Sunami T, Ichihashi N, Nishikawa T, Kazuta Y, and Yomo T (2016). Effect of Liposome Size on Internal RNA Replication Coupled with Replicase Translation. ChemBioChem 17, 1282–1289. 10.1002/cbic.201500662. [PubMed: 27037959]
8. Hilburger CE, Jacobs ML, Lewis KR, Peruzzi JA, and Kamat NP (2019). Controlling Secretion in Artificial Cells with a Membrane AND Gate. ACS Synthetic Biology 8, 1224–1230. 10.1021/acssynbio.8b00435. [PubMed: 31051071]
9. Zhang Y, Chen Y, Yang X, He X, Li M, Liu S, Wang K, Liu J, and Mann S (2021). Giant Coacervate Vesicles As an Integrated Approach to Cytomimetic Modeling. Journal of the American Chemical Society 143, 2866–2874. 10.1021/jacs.0c12494. [PubMed: 33566601]
10. Dewey DC, Strulson CA, Cacace DN, Bevilacqua PC, and Keating CD (2014). Bioreactor droplets from liposome-stabilized all-aqueous emulsions. Nature Communications 5, 4670. 10.1038/ncomms5670.
11. Lentini R, Santero SP, Chizzolini F, Cecchi D, Fontana J, Marchioretto M, Del Bianco C, Terrell JL, Spencer AC, Martini L, et al. (2014). Integrating artificial with natural cells to translate chemical messages that direct E. coli behaviour. Nature Communications 5, 4012. 10.1038/ncomms5012.
12. Chen IA, Roberts RW, and Szostak JW (2004). The emergence of competition between model protocells. Science 305, 1474–1476. 10.1126/science.1100757. [PubMed: 15353806]
13. Engelhart AE, Adamala KP, and Szostak JW (2016). A simple physical mechanism enables homeostasis in primitive cells. Nat. Chem 8, 448–453. 10.1038/nchem.2475 http://www.nature.eom/nchem/journal/v8/n5/abs/nchem.2475.html#supplementary-information. [PubMed: 27102678]
14. Black RA, Blosser MC, Stottrup BL, Tavakley R, Deamer DW, and Keller SL (2013). Nucleobases bind to and stabilize aggregates of a prebiotic amphiphile, providing a viable mechanism for the emergence of protocells. Proc. Natl. Acad. Sci. U. S. A 110, 13272–13276. 10.1073/pnas.1300963110. [PubMed: 23901105]
15. Saha R, Verbanic S, and Chen IA (2018). Lipid vesicles chaperone an encapsulated RNA aptamer. Nature Communications 9. 2313. 10.1038/s41467-018-04783-8.
16. Lai Y-C, Liu Z, and Chen IA (2021). Encapsulation of ribozymes inside model protocells leads to faster evolutionary adaptation. Proceedings of the National Academy of Sciences 118, e2025054118. 10.1073/pnas.2025054118.

17. Doudna JA, and Cech TR (2002). The chemical repertoire of natural ribozymes. Nature 418, 222–228. [PubMed: 12110898]

18. Paudel BP, and Rueda D (2014). Molecular Crowding Accelerates Ribozyme Docking and Catalysis. Journal of the American Chemical Society 136, 16700–16703. 10.1021/ja5073146. [PubMed: 25399908]

19. Strulson CA, Yennawar NH, Rambo RP, and Bevilacqua PC (2013). Molecular Crowding Favors Reactivity of a Human Ribozyme Under Physiological Ionic Conditions. Biochemistry 52, 8187–8197. 10.1021/bi400816s. [PubMed: 24187989]

20. Karimata H, Nakano S. i., and Sugimoto N (2006). The roles of cosolutes on the hammerhead ribozyme activity. Nucleic Acids Symposium Series 50, 81–82. 10.1093/nass/nrl040.

21. Nakano S. i., Karimata HT, Kitagawa Y, and Sugimoto N (2009). Facilitation of RNA Enzyme Activity in the Molecular Crowding Media of Cosolutes. Journal of the American Chemical Society 131, 16881–16888. 10.1021/ja9066628. [PubMed: 19874030]

22. Desai R, Kilburn D, Lee H-T, and Woodson SA (2014). Increased Ribozyme Activity in Crowded Solutions*. Journal of Biological Chemistry 289, 2972–2977. 10.1074/jbc.M113.527861.

23. Paudel BP, Fiorini E, Borner R, Sigel RKO, and Rueda DS (2018). Optimal molecular crowding accelerates group II intron folding and maximizes catalysis. Proceedings of the National Academy of Sciences 115, 11917–11922. 10.1073/pnas.1806685115.

24. Kilburn D, Roh JH, Guo L, Briber RM, and Woodson SA (2010). Molecular Crowding Stabilizes Folded RNA Structure by the Excluded Volume Effect. Journal of the American Chemical Society 132, 8690–8696. 10.1021/ja101500g. [PubMed: 20521820]

25. Kilburn D, Roh JH, Behrouzi R, Briber RM, and Woodson SA (2013). Crowders Perturb the Entropy of RNA Energy Landscapes to Favor Folding. Journal of the American Chemical Society 135, 10055–10063. 10.1021/ja4030098. [PubMed: 23773075]

26. Lee H-T, Kilburn D, Behrouzi R, Briber RM, and Woodson SA (2014). Molecular crowding overcomes the destabilizing effects of mutations in a bacterial ribozyme. Nucleic Acids Research 43, 1170–1176. 10.1093/nar/gku1335. [PubMed: 25541198]

27. Rahman MS, Gulshan MA, Matsumura S, and Ikawa Y (2020). Polyethylene glycol molecular crowders enhance the catalytic ability of bimolecular bacterial RNase P ribozymes. Nucleosides, Nucleotides & Nucleic Acids 39, 715–729. 10.1080/15257770.2019.1687909.

28. Strulson CA, Molden RC, Keating CD, and Bevilacqua PC (2012). RNA catalysis through compartmentalization. Nature Chemistry 4, 941–946. 10.1038/nchem.1466.

29. Zhou H-X, and Dill KA (2001). Stabilization of Proteins in Confined Spaces. Biochemistry 40, 11289–11293. 10.1021/bi0155504. [PubMed: 11560476]

30. Feldstein PA, Buzayan JM, and Bruening G (1989). Two sequences participating in the autolytic processing of satellite tobacco ringspot virus complementary RNA. Gene 82, 53–61. 10.1016/0378-1119(89)90029-2. [PubMed: 2583519]

31. Hampel A, and Tritz R (1989). RNA catalytic properties of the minimum (−)sTRSV sequence. Biochemistry 28, 4929–4933. 10.1021/bi00438a002. [PubMed: 2765519]

32. Wilson TJ, Nahas M, Araki L, Harusawa S, Ha T, and Lilley DMJ (2007). RNA folding and the origins of catalytic activity in the hairpin ribozyme. Blood Cells, Molecules, and Diseases 38, 8–14. 10.1016/j.bcmd.2006.10.004.

33. Murchie AIH, Thomson JB, Walter F, and Lilley DMJ (1998). Folding of the Hairpin Ribozyme in Its Natural Conformation Achieves Close Physical Proximity of the Loops. Molecular Cell 1, 873–881. 10.1016/S1097-2765(00)80086-6. [PubMed: 9660970]

34. Zhuang X, Kim H, Pereira MJB, Babcock HP, Walter NG, and Chu S (2002). Correlating Structural Dynamics and Function in Single Ribozyme Molecules. Science 296, 1473–1476. 10.1126/science.1069013. [PubMed: 12029135]

35. van Tol H, Buzayan JM, Feldstein PA, Eckstein F, and Bruening G (1990). Two autolytic processing reactions of a satellite RNA proceed with inversion of configuration. Nucleic Acids Research 18, 1971–1975. 10.1093/nar/18.8.1971. [PubMed: 1692411]

36. Pinard R, Lambert D, Walter NG, Heckman JE, Major F, and Burke JM (1999). Structural Basis for the Guanosine Requirement of the Hairpin Ribozyme. Biochemistry 38, 16035–16039. 10.1021/bi992024s. [PubMed: 10587425]

37. Gaur S, Heckman JE, and Burke JM (2008). Mutational inhibition of ligation in the hairpin ribozyme: Substitutions of conserved nucleobases A9 and A10 destabilize tertiary structure and selectively promote cleavage. RNA 14, 55–65. 10.1261/rna.716108. [PubMed: 17998292]
38. Liu S, Bokinsky G, Walter NG, and Zhuang X (2007). Dissecting the multistep reaction pathway of an RNA enzyme by single-molecule kinetic “fingerprinting”. Proceedings of the National Academy of Sciences 104, 12634–12639. 10.1073/pnas.0610597104.
39. Walter NG (2001). Structural Dynamics of Catalytic RNA Highlighted by Fluorescence Resonance Energy Transfer. Methods 25, 19–30. 10.1006/meth.2001.1212. [PubMed: 11558994]
40. Hanczyc MM, Fujikawa SM, and Szostak JW (2003). Experimental models of primitive cellular compartments: Encapsulation, growth, and division. Science 302, 618–622. 10.1126/science.1089904. [PubMed: 14576428]
41. Zhu TF, and Szostak JW (2009). Coupled growth and division of model protocell membranes. J. Am. Chem. Soc 131, 5705–5713. 10.1021/ja900919c. [PubMed: 19323552]
42. Joyce GF, and Szostak JW (2018). Protocells and RNA Self-Replication. Cold Spring Harb Perspect Biol 10. 10.1101/cshperspect.a034801.
43. Deamer DW, and Dworkin JP (2005). Chemistry and Physics of Primitive Membranes. In Prebiotic Chemistry, Walde P, ed. (Springer Berlin Heidelberg), pp. 1–27. 10.1007/bl36806.
44. Jin L, Kamat NP, Jena S, and Szostak JW (2018). Fatty Acid/Phospholipid Blended Membranes: A Potential Intermediate State in Protocellular Evolution. Small 14, 1704077. 10.1002/smll.201704077.
45. Appel B, Marschall T, Strahl A, and Miiller S (2012). Kinetic Characterization of Hairpin Ribozyme Variants. In Ribozymes: Methods and Protocols, Hartig JS, ed. (Humana Press), pp. 41–59. 10.1007/978-1-61779-545-9_4.
46. Chen IA, Salehi-Ashtiani K, and Szostak JW (2005). RNA catalysis in model protocell vesicles. Journal of the American Chemical Society 127, 13213–13219. 10.1021/ja051784p. [PubMed: 16173749]
47. Gao M, Arns L, and Winter R (2017). Modulation of the Thermodynamic Signatures of an RNA Thermometer by Osmolytes and Salts. Angewandte Chemie International Edition 56, 2302–2306. 10.1002/anie.201611843. [PubMed: 28102930]
48. Idili A, Vallee-Belisle A, and Ricci F (2014). Programmable pH-Triggered DNA Nanoswitches. Journal of the American Chemical Society 136, 5836–5839. 10.1021/ja500619w. [PubMed: 24716858]
49. Ashton NW, Bolderson E, Cubeddu L, O’Byrne KJ, and Richard DJ (2013). Human single-stranded DNA binding proteins are essential for maintaining genomic stability. BMC Molecular Biology 14, 9. 10.1186/1471-2199-14-9. [PubMed: 23548139]
50. Maffeo C, and Aksimentiev A (2017). Molecular mechanism of DNA association with single-stranded DNA binding protein. Nucleic Acids Research 45, 12125–12139. 10.1093/nar/gkx917. [PubMed: 29059392]
51. Gao M, Gnutt D, Orban A, Appel B, Righetti F, Winter R, Narberhaus F, Miiller S, and Ebbinghaus S (2016). RNA Hairpin Folding in the Crowded Cell. Angewandte Chemie International Edition 55, 3224–3228. 10.1002/anie.201510847. [PubMed: 26833452]
52. Zimmerman SB, and Trach SO (1988). Effects of macromolecular crowding on the association of E.coli ribosomal particles. Nucleic Acids Research 16, 6309–6326. 10.1093/nar/16.14.6309. [PubMed: 3041372]
53. Dupuis NF, Flolmstrom ED, and Nesbitt DJ (2014). Molecular-crowding effects on single-molecule RNA folding/unfolding thermodynamics and kinetics. Proceedings of the National Academy of Sciences 111, 8464–8469. 10.1073/pnas.1316039111.
54. Lambert D, and Draper DE (2007). Effects of Osmolytes on RNA Secondary and Tertiary Structure Stabilities and RNA-Mg2+ Interactions. Journal of Molecular Biology 370, 993–1005. 10.1016/j.jmb.2007.03.080. [PubMed: 17555763]
55. Nakano S. i., Karimata H, Ohmichi T, Kawakami J, and Sugimoto N (2004). The Effect of Molecular Crowding with Nucleotide Length and Cosolute Structure on DNA Duplex Stability. Journal of the American Chemical Society 126, 14330–14331. 10.1021/ja0463029. [PubMed: 15521733]

56. Spink CH, and Chaires JB (1999). Effects of Hydration, Ion Release, and Excluded Volume on the Melting of Triplex and Duplex DNA. Biochemistry 38, 496–508. 10.1021/bi9820154. [PubMed: 9890933]
57. Nakano S. i., Yamaguchi D, Tateishi-Karimata H, Miyoshi D, and Sugimoto N (2012). Hydration Changes upon DNA Folding Studied by Osmotic Stress Experiments. Biophysical Journal 102, 2808–2817. 10.1016/j.bpj.2012.05.019. [PubMed: 22735531]
58. Rozners E, and Moulder J (2004). Hydration of short DNA, RNA and 2′ - OMe oligonucleotides determined by osmotic stressing. Nucleic Acids Research 32, 248–254. 10.1093/nar/gkh175. [PubMed: 14715922]
59. Schuabb C, Kumar N, Pataraia S, Marx D, and Winter R (2017). Pressure modulates the self-cleavage step of the hairpin ribozyme. Nature Communications 8, 14661. 10.1038/ncomms14661.
60. John SantaLucia J, and Hicks D (2004). The Thermodynamics of DNA Structural Motifs. Annual Review of Biophysics and Biomolecular Structure 33, 415–440. 10.1146/annurev.biophys.32.110601.141800.
61. Sugimoto N (2014). Chapter Eight - Noncanonical Structures and Their Thermodynamics of DNA and RNA Under Molecular Crowding: Beyond the Watson–Crick Double Helix. In International Review of Cell and Molecular Biology, Hancock R, and Jeon KW, eds. (Academic Press), pp. 205–273. 10.1016/B978-0-12-800046-5.00008-4.
62. Eigen M (1971). Self-organization of matter and the evolution of biological macromolecules. Naturwissenschaften 58, 465–523. 10.1007/BF00623322. [PubMed: 4942363]
63. Kun Á, Santos M, and Szathmáry E (2005). Real ribozymes suggest a relaxed error threshold. Nature Genetics 37, 1008–1011. 10.1038/ngl621. [PubMed: 16127452]
64. Lincoln TA, and Joyce GF (2009). Self-Sustained Replication of an RNA Enzyme. Science 323, 1229–1232. 10.1126/science.1167856. [PubMed: 19131595]
65. Vaidya N, Manapat ML, Chen IA, Xulvi-Brunet R, Hayden EJ, and Lehman N (2012). Spontaneous network formation among cooperative RNA replicators. Nature 491, 72–77. 10.1038/nature11549. [PubMed: 23075853]
66. Doudna JA, and Cech TR (1995). Self-assembly of a group I intron active site from its component tertiary structural domains. RNA 1, 36–45. [PubMed: 7489486]
67. Tjhung KF, Shokhirev MN, Horning DP, and Joyce GF (2020). An RNA polymerase ribozyme that synthesizes its own ancestor. Proceedings of the National Academy of Sciences 117, 2906–2913. 10.1073/pnas.1914282117.
68. Wachowius F, and Holliger P (2019). Non-Enzymatic Assembly of a Minimized RNA Polymerase Ribozyme. ChemSystemsChem 1, 1–4. 10.1002/syst.201900004. [PubMed: 31673682]
69. Fujikawa SM, Chen IA, and Szostak JW (2005). Shrink-Wrap Vesicles. Langmuir 21, 12124–12129. 10.1021/la052590q. [PubMed: 16342983]
70. ÖSTLING S, and VIRTAMA P (1946). A Modified Preparation of the Universal Buffer Described by Teorell and Stenhagen. Acta Physiologica Scandinavica 11, 289–293. 10.1111/j.1748-1716.1946.tb00349.x.
71. Rublack N, Nguyen H, Appel B, Springstubbe D, Strohbach D, and Müller S (2011). Synthesis of Specifically Modified Oligonucleotides for Application in Structural and Functional Analysis of RNA. Journal of Nucleic Acids 2011, 805253. 10.4061/2011/805253. [PubMed: 22013508]
72. Hegg LA, and Fedor MJ (1995). Kinetics and Thermodynamics of Intermolecular Catalysis by Hairpin Ribozymes. Biochemistry 34, 15813–15828. 10.1021/bi00048a027. [PubMed: 7495813]
73. Nesbitt SM, Erlacher HA, and Fedor MJ (1999). The internal equilibrium of the hairpin ribozyme: temperature, ion and pH effects. Journal of Molecular Biology 286, 1009–1024. 10.1006/jmbi.1999.2543. [PubMed: 10047478]
74. Donahue CP, Yadava RS, Nesbitt SM, and Fedor MJ (2000). The kinetic mechanism of the hairpin ribozyme in vivo: influence of RNA helix stability on intracellular cleavage kinetics11Edited by D. E. Draper. Journal of Molecular Biology 295, 693–707. 10.1006/jmbi.1999.3380. [PubMed: 10623557]
75. Nahas MK, Wilson TJ, Hohng S, Jarvie K, Lilley DMJ, and Ha T (2004). Observation of internal cleavage and ligation reactions of a ribozyme. Nature Structural & Molecular Biology 11, 1107–1113. 10.1038/nsmb842.

Highlights

- Encapsulation enhances the cleavage and ligation activities of hairpin ribozymes.
- Encapsulation promotes RNA-RNA association and DNA triplex structures.
- Encapsulation rescues the activity of folding-deficient hairpin ribozyme mutants.

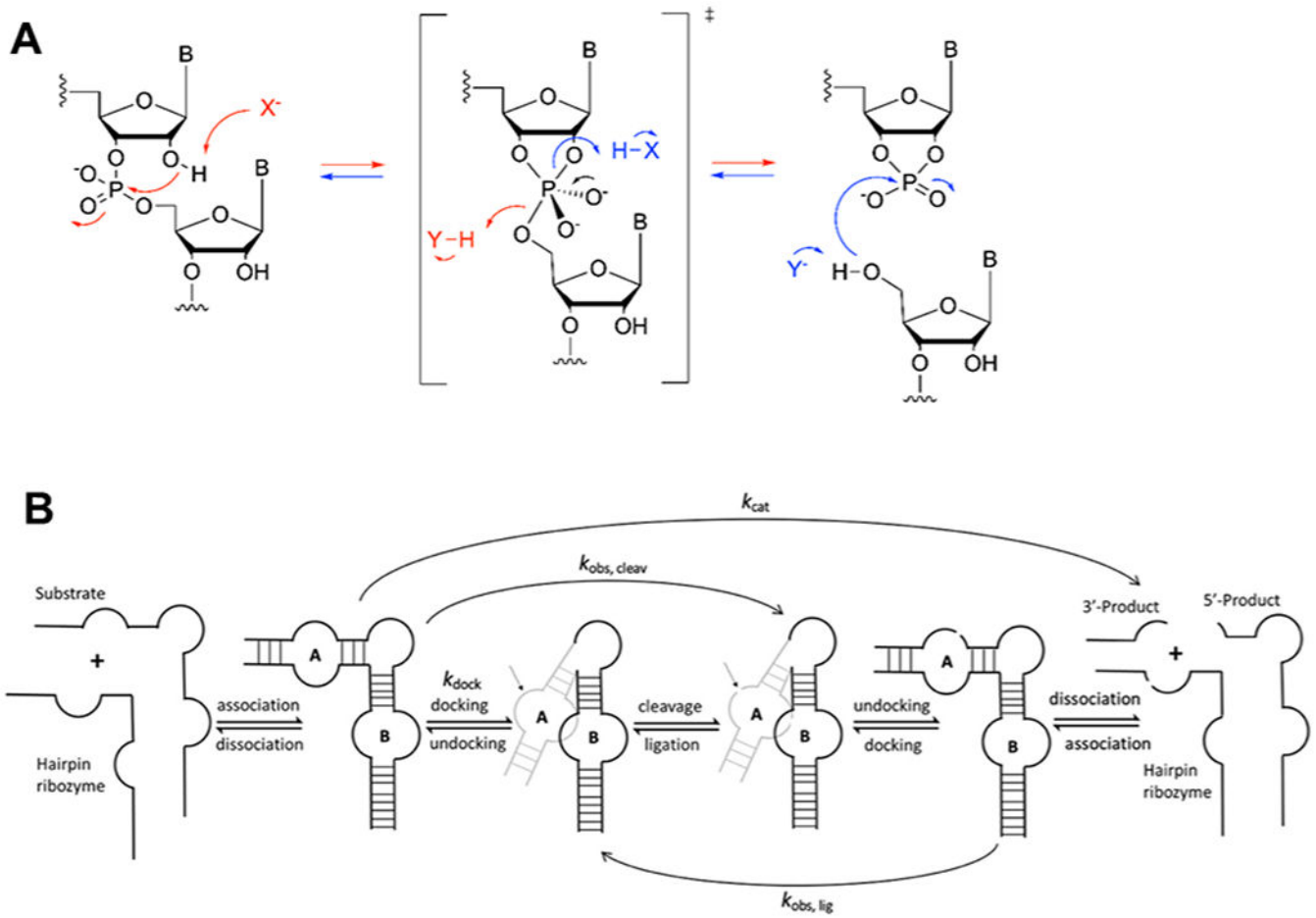

Figure 1. Catalysis by the hairpin ribozyme.

(A) Reaction mechanism of the hairpin ribozyme (red: cleavage; blue: ligation). (B) Folding pathway of the hairpin ribozyme (adapted from [34]). Measured parameters correspond to steps as indicated. Note that $k_{obs,cleav}$ includes the docking and cleavage steps.

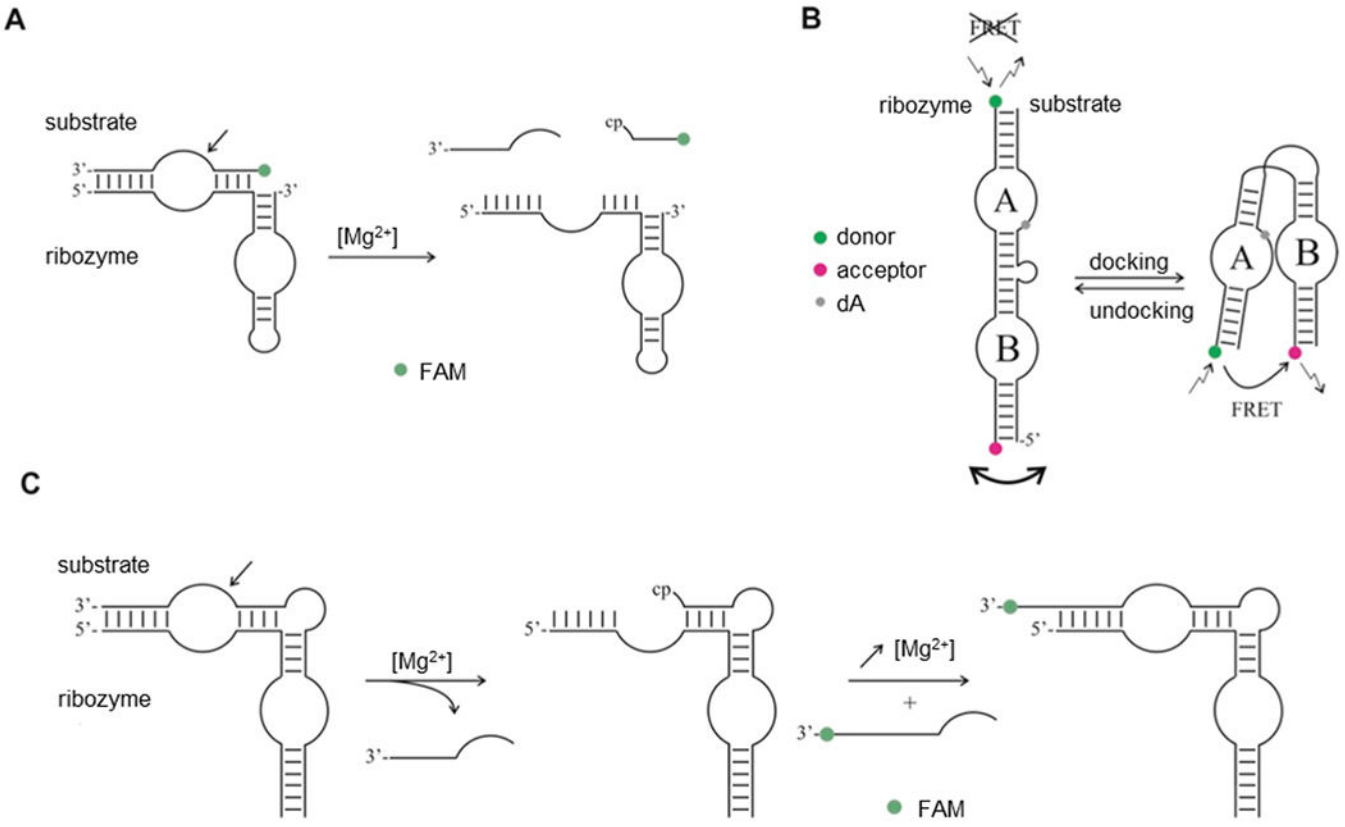

Figure 2. Assays of hairpin ribozyme activity and folding.

(A) Cleavage of a fluorescently labelled substrate releases a fluorescent product that can be quantified by gel electrophoresis. (B) Adoption of the docked conformation brings a FRET pair into close proximity, generating a signal. Adenosine at the cleavage site in loop A was replaced by its deoxy analogue (dA) to prevent cleavage. (C) In general, ligation-competent ribozyme-substrate complex is prepared by annealing the ribozyme strand with a cleavage substrate and conducting the cleavage reaction at 7 mM Mg^{2+}. Dissociation of the smaller 3' cleavage product results in the ribozyme strand in complex with the 5' ligation substrate strand carrying the required 2′,3′- cyclic phosphate (labeled 'cp'). Then, addition of a fluorescently labeled 3' substrate strand and higher [Mg^{2+}] allows assessment of ligation activity by gel electrophoresis.

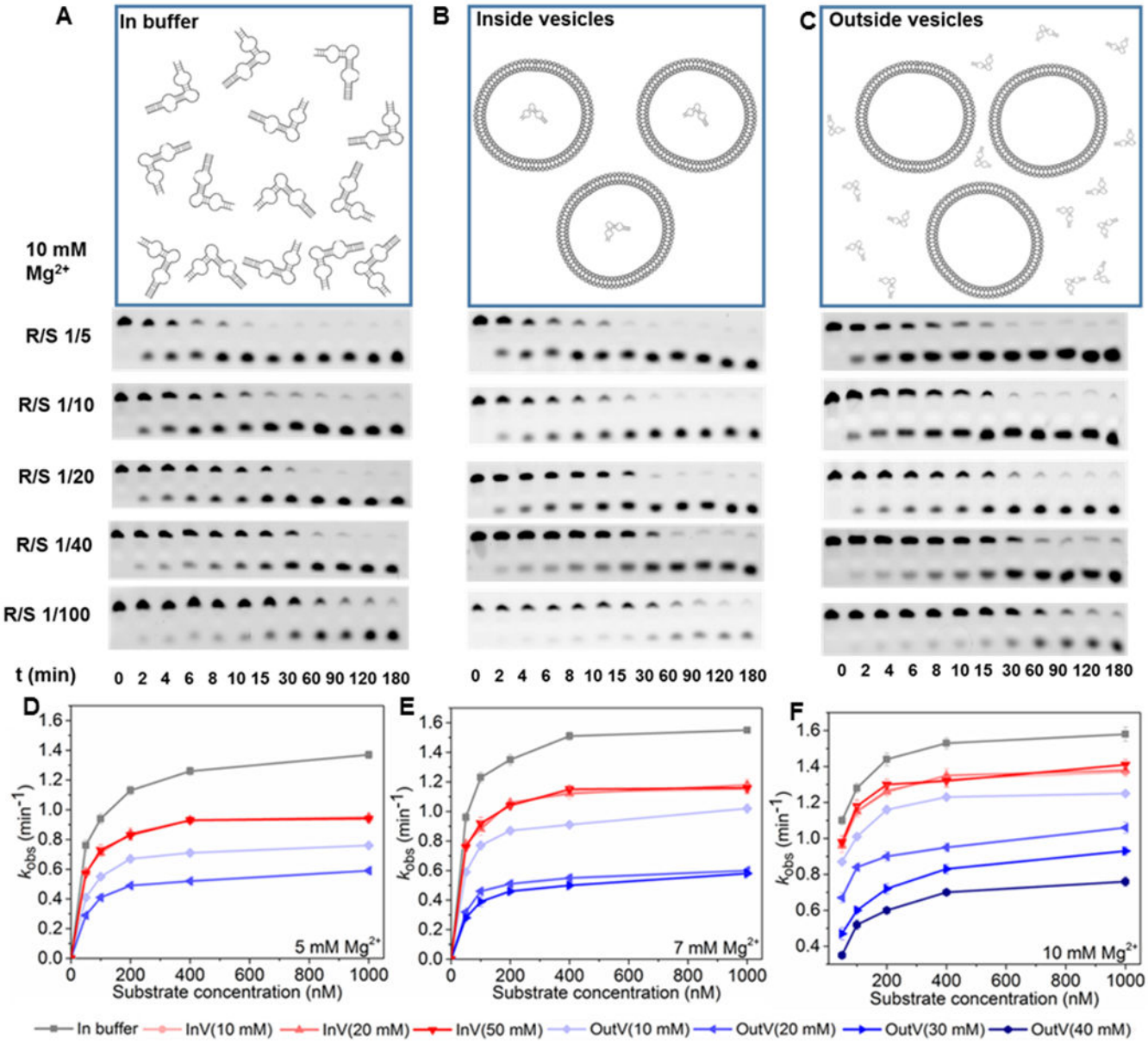

Figure 3. Gel assay following product formation from the hairpin ribozyme using substrate RNA and Michaelis-Menten plots of the hairpin ribozyme reaction.

(A-C) Shown here are representative gels demonstrating the cleavage reaction at time intervals (t = 0, 2, 4, 6, 8, 10, 15, 30, 60, 90, 120, and 180 min) under different conditions: (A) in buffer, (B) encapsulated inside vesicles (InV), and (C) exposed to empty vesicles (OutV). In this experiment, [Mg^{2+}] = 10 mM, and the ribozyme/substrate ratios (R/S) are 1/5, 1/10, 1/20, 1/40, 1/100. The lipid concentration in the assays shown is 10 mM. See Figure 2A. (D-F) Michaelis-Menten plots of the hairpin ribozyme reaction in the presence of excess substrate RNA, with reaction rate k_{obs} vs. [substrate], for 5 mM (D), 7 mM (E), or 10 mM (F) Mg^{2+}. Conditions were in lipid-free buffer (gray), encapsulated in vesicles (red, with [lipid] as indicated), or outside vesicles (blue, with [lipid] as indicated). Standard

deviations from at least three replicates are shown by error bars. See also Figure 2A, S1–3, Table S5–6.

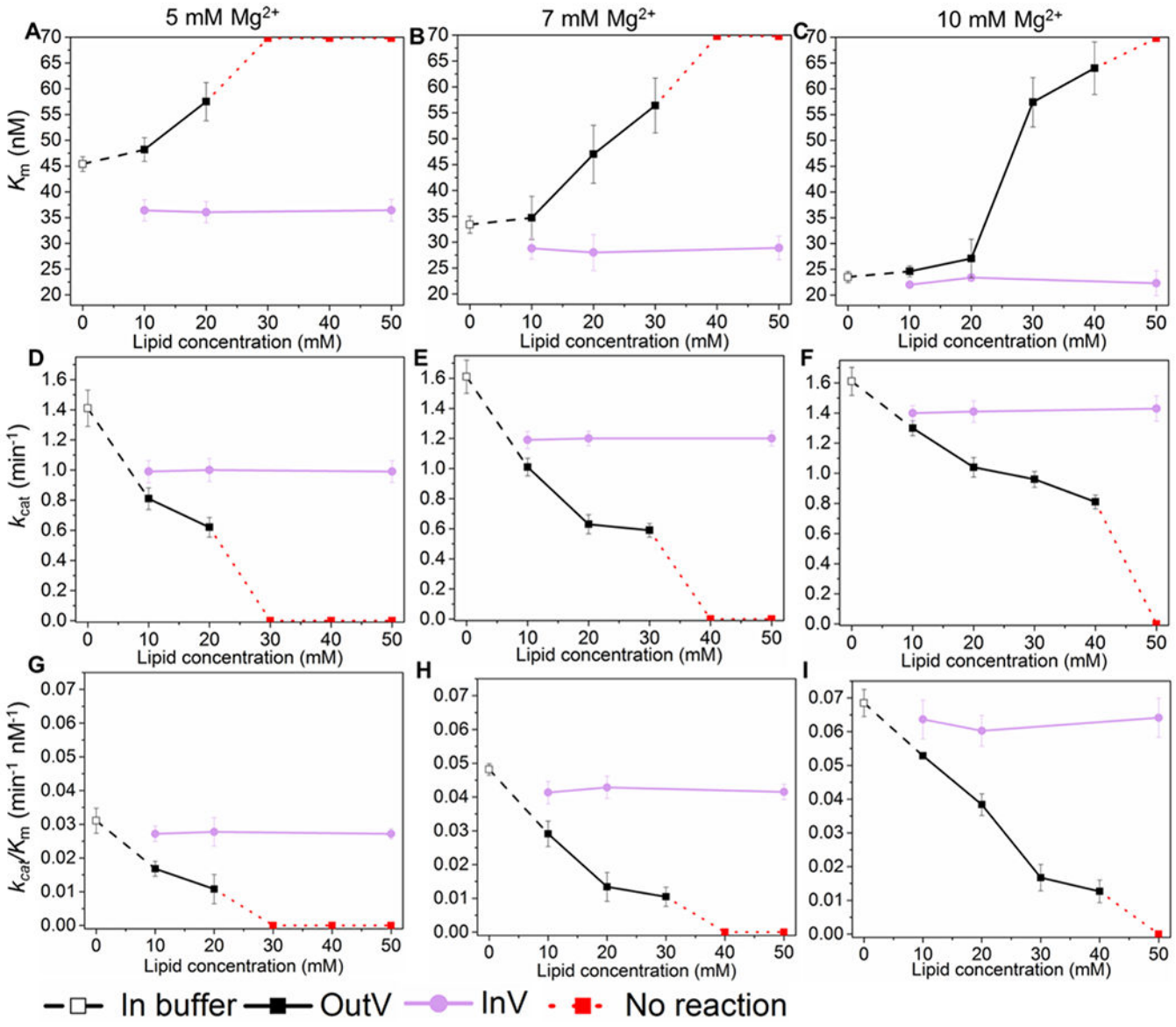

Figure 4. Dependence of K_m (A-C), k_{cat} (D-F), and k_{cat}/K_m (G-I) of the hairpin ribozyme cleavage reaction on lipid concentration, in the presence of 5, 7, or 10 mM Mg^{2+} (left, middle, and right columns, respectively), under multiple-turnover conditions.

The ribozyme and substrate RNA are either in buffer without lipids (black open squares; lipid concentration = 0), exposed to empty vesicles (OutV, black squares) or encapsulated inside vesicles (InV, purple circles). Red markers and dotted lines at the top (for K_m) or bottom (for k_{cat} and k_{cat}/K_m) of the horizontal axes indicate reactions for which no product was detected (Figure S4I). Each point is an average of three replicates, with error bars showing standard deviation. See also Figure 2A, S1–4, Table S5–6.

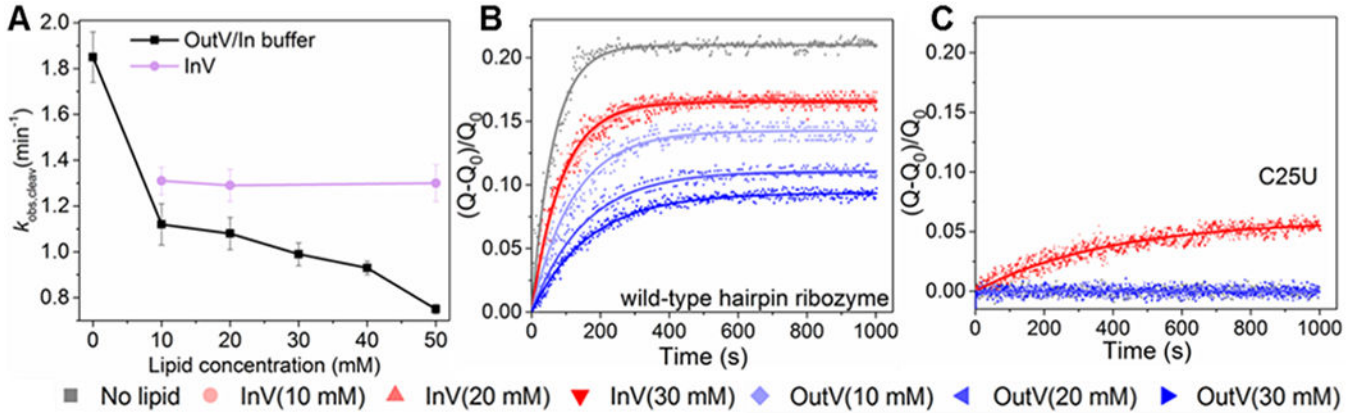

Figure 5. Dependence of the single-turnover hairpin ribozyme cleavage reaction ($k_{obs,cleav}$) on lipid concentration, and FRET study of mutants.

(a) Reactions were conducted with a ribozyme:substrate ratio of 10:1 and in the presence of 5 mM Mg^{2+}. The ribozyme and substrate RNA are either in buffer without lipids (black square; lipid concentration = 0), exposed to empty vesicles (OutV, black squares with lines) or encapsulated inside vesicles (InV, purple circles with lines). Each point is an average of three replicates, with error bars showing standard deviation. See Figure 2A. (B, C) Ribozyme docking measured by FRET for the hairpin ribozyme in lipid-free solution (gray), exposed to empty vesicles (blue; lipid concentration indicated), or encapsulated in vesicles (red; lipid concentration indicated). Docking of the wild-type (B) and the mutant C25U (C) are shown with substrate RNA **5.** Note that all conditions were tested in (C), and the lipid-free condition and all OutV conditions showed baseline FRET during the experiment. Relative FRET efficiency was calculated as a normalized ratio of acceptor to donor fluorescence (Q), i.e., $(Q\text{-}Q_0)/Q_0$, where (Q_0 is the initial value of Q. The docking rate was determined by nonlinear least-squares fitting to the equation $Q = Q_A\,(1–e^{-k_{dock}*t})$ where Q_A is the amplitude of the signal and k_{dock} is the rate constant. See also Figure 2, S4–5, and Table S2.

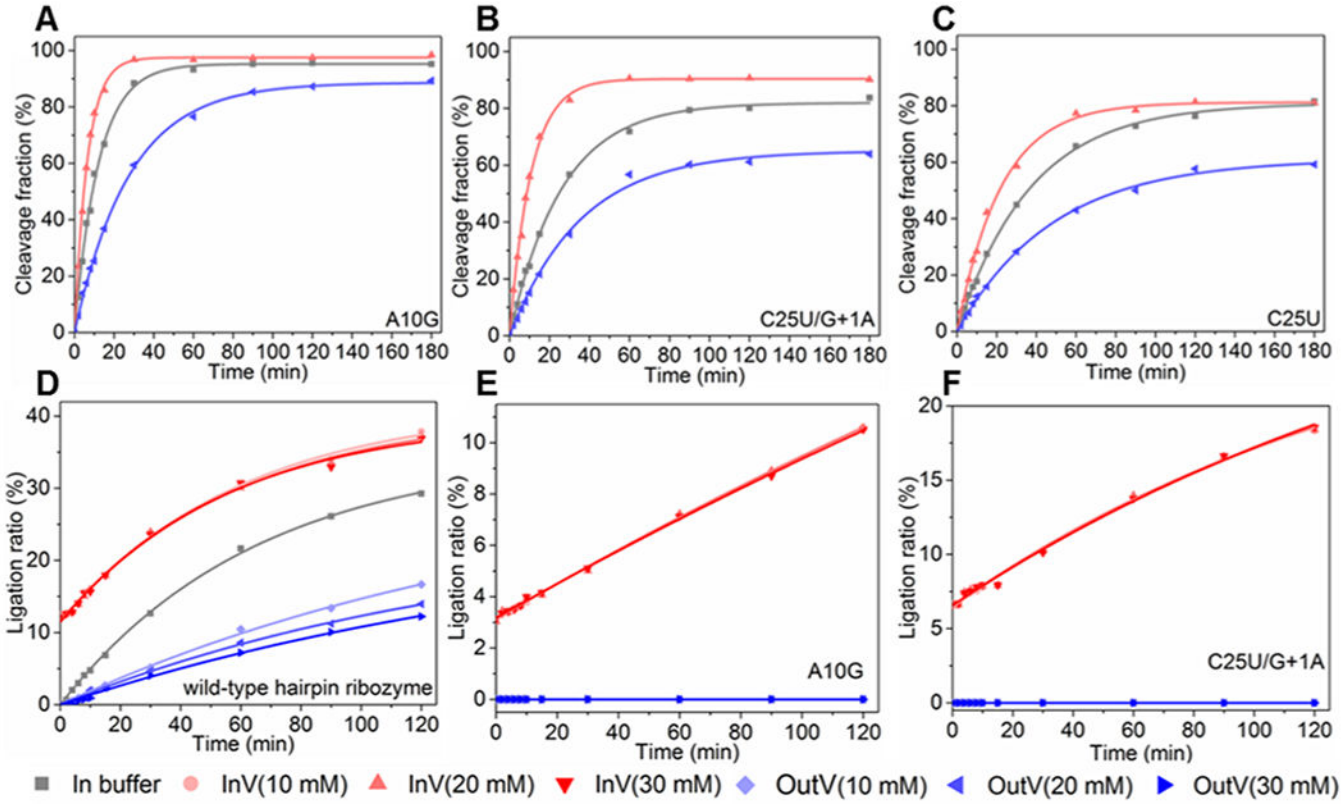

Figure 6. Cleavage and ligation activity of folding-deficient hairpin ribozyme mutants.

(A, B, C) Kinetics of the multiple-turnover cleavage reaction ([ribozyme mutant]/[substrate] ratio = 1/20) in the presence of 5 mM Mg^{2+} for the three folding-deficient mutants: (A) A10G, (B) C25U (with substrate G+1A) and (C) C25U. The lipid concentrations of the vesicles are 20 mM for cleavage reactions in the InV and OutV conditions. See Figure 2A. (D, E, F) Kinetics of the ligation reaction with ribozyme/substrate ratio of 1/1 in the presence of 10 mM Mg^{2+}, for the wild-type hairpin ribozyme (D), mutant A10G (E) and C25U (substrate G+1A) (F). For reactions with lipids, the concentration of the vesicles was 10, 20, or 30 mM, as indicated in the legend. In (E-F), the gray line for reaction in lipid-free buffer is present at approximately baseline throughout the experiment. Note that some ligation is present at time ‘zero’ for the encapsulated reaction (D-F), as some ligation occurred during incubation at the lower [Mg^{2+}] used to prepare the ligation-competent ribozyme (Figure 2C; STAR Methods). Solid lines are curve fits to a single exponential equation (see Table S4, Section 1). See also Figure 2, S6, Table S3–4.

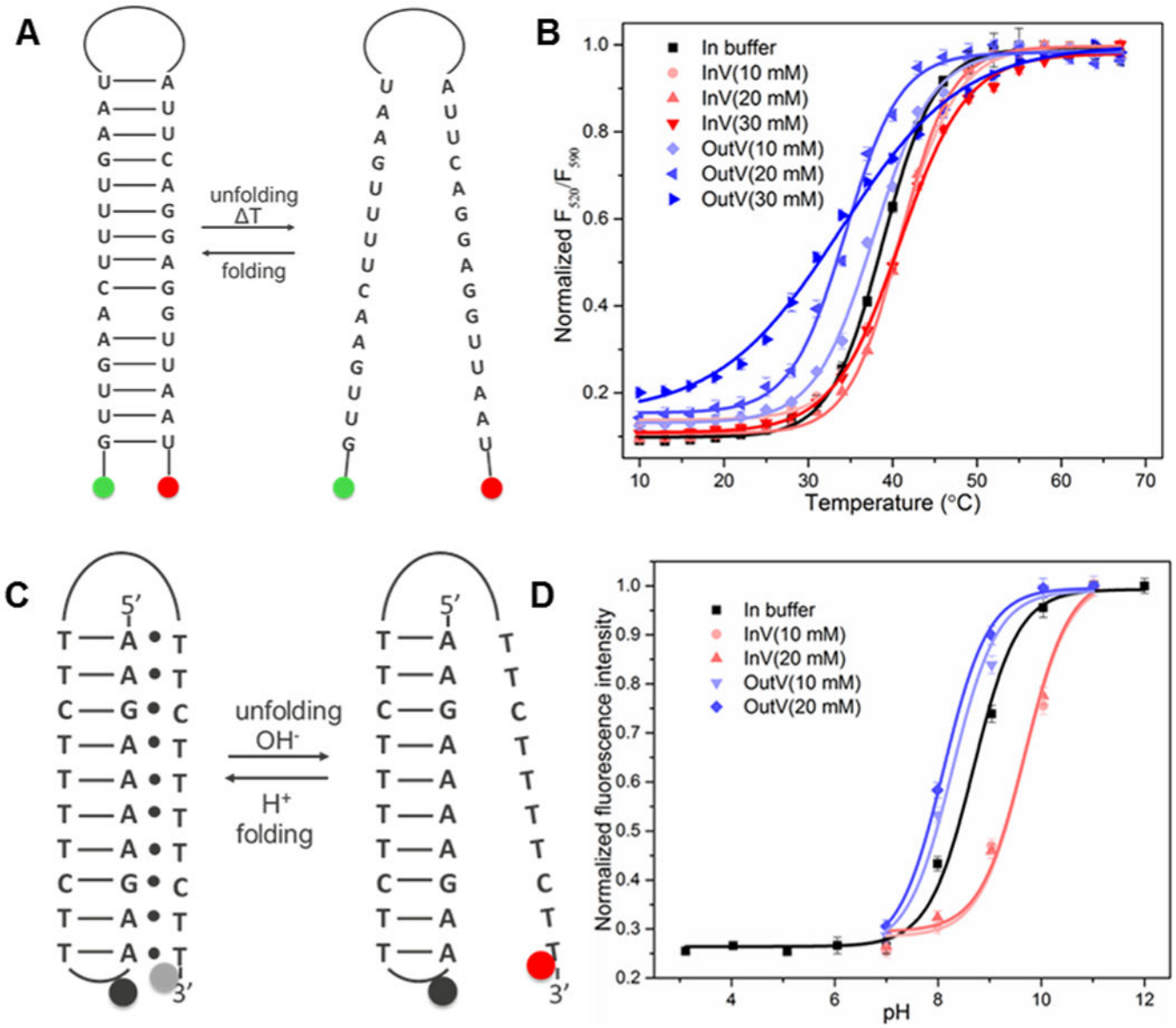

Figure 7. Effect of encapsulation on secondary structure formation of RNA and DNA.

(A, B) Melting of an RNA stem-loop structure monitored by FRET. (A) Structure of the stem-loop RNA; (B) the FRET-based melting curves of the stem-loop RNA (ratio of donor emission fluorescence (λ=520 nm) to acceptor emission fluorescence (λ=590 nm), normalized to 1), in the absence of vesicles (in buffer, black), inside vesicles (InV, red) and outside vesicles (OutV, blue). The lipid concentrations of the vesicles are 10, 20 or 30 mM as indicated. Error bars indicate standard deviation of three replicates (Table S4, Section 3). See Figure S7A–G for fluorescence spectra. (C, D) A triplex DNA switch is denatured to duplex structure by increasing pH, releasing fluorescence quenching. (C) Structure of the triplex DNA switch. (D) Fluorescence (λ_{ex} = 488 nm, λ_{em} λ = 572 nm) was measured at different pH, resulting in titration curves in the following conditions: in the absence of vesicles (black), inside vesicles (InV, red) and outside vesicles (OutV, blue).

The lipid concentrations of the vesicles are 10 and 20 mM, as labeled. Three replicates were performed for each measurement. See also Figure S7 and Table S4.

KEY RESOURCES TABLE

REAGENT or RESOURCE	SOURCE	IDENTIFIER
Chemicals, peptides, and recombinant proteins		
Phospholipid POPC	Avanti Polar Lipids	Catalog #: 850457C-25mg
Sepharose 4B	Millipore Sigma	Catalog #: 4B200-100ML
oleic acid	Millipore Sigma	Catalog #: O1008
methanol	VWR	Catalog #: BDH1135-1LP
Klenow Fragment, exo–	Thermo Fisher	Catalog #: EP0421
DNase I	Thermo Fisher Scientific	Catalog #: 18047019
Triton™ X-100	Millipore Sigma	Catalog #: T8787-50ML
Deoxynucleotide (dNTP) Solution Mix	New England Biolabs	Catalog #: N0447S
Magnesium chloride	Millipore Sigma	Catalog #: M8266-100G
Urea	Millipore Sigma	Catalog #: U5378-100G
Critical commercial assays		
HiScribe™ T7 High Yield RNA Synthesis Kit	New England Biolabs	Catalog #: E2040S
ADIFAB Kits	FFA Sciences	Catalog #: ADI-1-200
Oligonucleotides		
5′ -(FAM)CUC ACA GUC CUC UUU-3′	This paper order from IDT	N/A
5′ -(FAM)CUC ACA AUC CUC UUU-3′	This paper order from IDT	N/A
5′-(Atto488)GUU GAA CUU UUG AAU AGU GAU UCA GGA GGU UAAU(Atto565)-3′	This paper order from IDT	N/A
5′ -TAA TAC GAC TCA CTA TAG GGA GAA AGA GAG AAG TGA ACC AGA GAA A-3′	This paper order from IDT	N/A
5′ -TAC CAG GTA ATA TAC CAC AAC GTG TGT TTC TCT GGT TCA CTT CTC T-3′	This paper order from IDT	N/A
5′ -TAA TAC GAC TCA CTA TAG GGA GAA AGA GAG AAG TGA ACC AGA GAA A-3′	This paper order from IDT	N/A
5′ -TAC CAG GTA ATA TAC CAC AAC GTG TAT TTC TCT GGT TCA CTT CTC T-3′	This paper order from IDT	N/A
5′ -TAA TAC GAC TCA CTA TAG GGA GAA AGA GAG AGG TGA ACC AGA GAA A-3′	This paper order from IDT	N/A
5′ -TAC CAG GTA ATA TAC CAC AAC GTG TGT TTC TCT GGT TCA CTT CTC T-3′	This paper order from IDT	N/A
5′ -AAGAA-AAGAA-TTT(BHQ-2)A-TTCTT-TTCTT-CTTTG-TTCTT-TTCTT(AF546)-3′	This paper order from IDT	N/A
Software and algorithms		
OriginPro 2015	OriginLab Corporation	https://www.originlab.com/2015
ChemDraw Professional 18.0	PerkinElmer	https://www.perkinelmer.com/category/chemdraw
Other		
TECAN infinite 200 Pro plate reader	TECAN	https://lifesciences.tecan.com/plate_readers/infinite_200_pro
Amersham™ Typhoon™ RGB	GE Healthcare	https://www.cytivalifesciences.com/en/us/shop/protein-analysis/molecular-imaging-for-proteins/imaging-systems/amersham-typhoon-gel-and-blot-imaging-systems-p-00192

REAGENT or RESOURCE	SOURCE	IDENTIFIER
Fluoromax 4C	Horiba	https://www.horiba.com/en_en/products/detail/action/show/Product/fluoromax-1576/